iScience

CellPress
OPEN ACCESS

Article

Minichromosome maintenance 6 protects against renal fibrogenesis by regulating DUSP6-mediated ERK/GSK-3β/Snail1 signaling

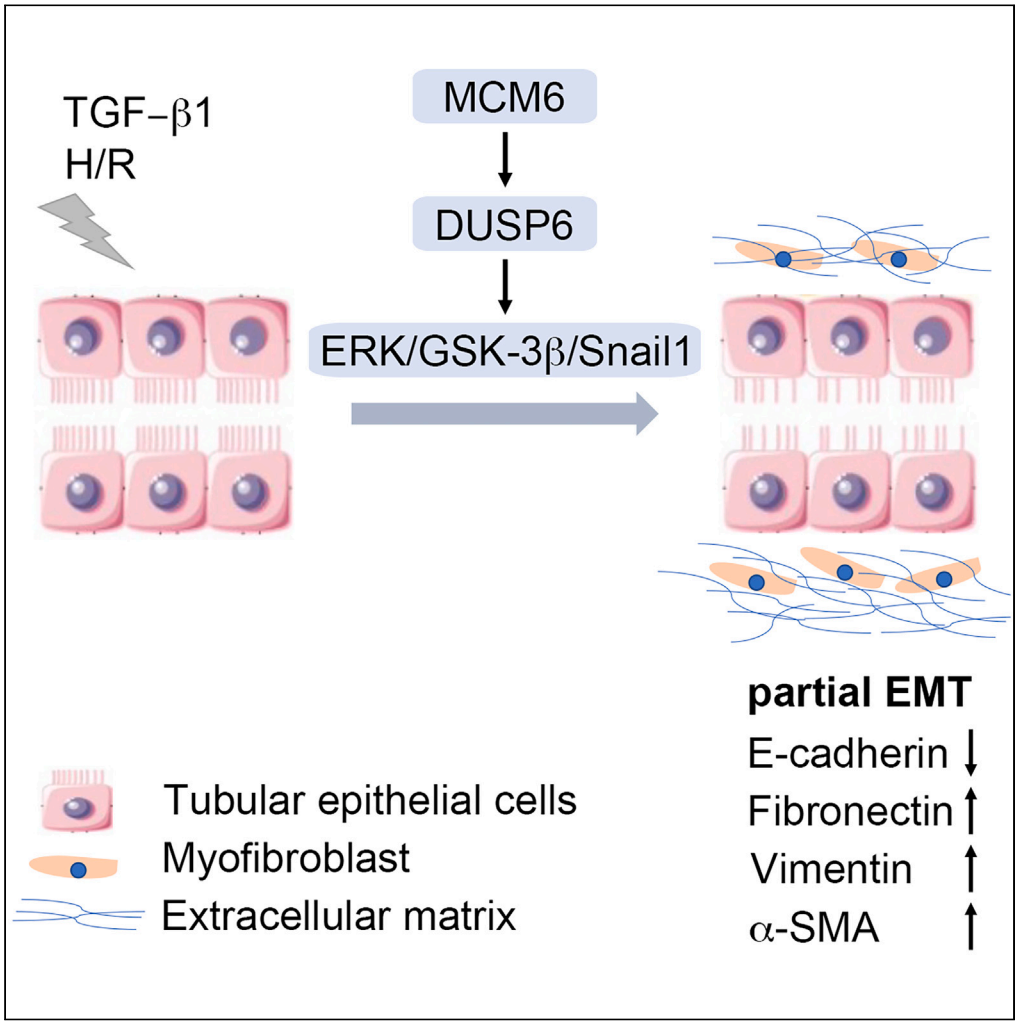

Jing Huang, Zhi-Feng Xu, Feng Liu, An-Ni Song, Hua Su, Chun Zhang

drzhangchun@hust.edu.cn

Highlights

Tubular injury triggers the upregulation of MCM6 in proximal TECs

DUSP6 expression is substantially decreased in fibrotic kidneys

MCM6 contributes to the activation of DUSP6-mediated ERK/GSK-3β/Snail1 signaling

MCM6 level is crucial for tubular partial EMT and renal fibrogenesis

Huang et al., iScience 26, 107940
October 20, 2023
https://doi.org/10.1016/j.isci.2023.107940

iScience

CellPress
OPEN ACCESS

Article

Minichromosome maintenance 6 protects against renal fibrogenesis by regulating DUSP6-mediated ERK/GSK-3β/Snail1 signaling

Jing Huang,[1] Zhi-Feng Xu,[1] Feng Liu,[1] An-Ni Song,[1] Hua Su,[1] and Chun Zhang[1,2,*]

SUMMARY

Minichromosome maintenance 6 (MCM6) has been implicated in the progression of various malignant tumors; however, its exact physiological function in kidney diseases remains unclear. Here, we demonstrated that MCM6 levels showed a significant increase in the proximal tubular cells during progressive renal fibrosis in two unrelated *in vivo* fibrotic models, including unilateral ureteral obstruction (UUO) and unilateral ischemia-reperfusion injury (UIRI). Depletion of MCM6 aggravated partial epithelial-mesenchymal transition, extracellular matrix accumulation, and myofibroblast activation in the kidneys of UUO or UIRI mice. Conversely, overexpression of MCM6 promoted the recovery of E-cadherin and retarded UUO- or UIRI-induced renal fibrosis. In addition, DUSP6 expression substantially decreased in fibrotic kidneys, and it might be involved in MCM6-induced renal fibrosis by regulating the activation of ERK/GSK-3β/Snail1 signaling. In conclusion, our results highlight the significance of MCM6 in renal fibrosis, providing a potential therapeutic target for patients with chronic kidney disease.

INTRODUCTION

Chronic kidney disease (CKD) is a clinical syndrome characterized by persistent urinary and structural abnormalities or impaired excretory renal function with a high prevalence and eventual progression to end-stage renal disease.[1] Renal fibrosis is a pathological process characterized by abnormal activation of myofibroblasts, excessive deposition of extracellular matrix (ECM) in the interstitium, and destruction of the normal kidney architecture as an inevitable outcome in all types of progressive CKD.[2,3] Renal tubulointerstitial fibrosis (TIF), which is characterized by epithelial-to-mesenchymal transition (EMT) of renal tubular epithelial cells (TECs) and excessive deposition of ECM, is a crucial pathological factor of renal fibrosis.[4] EMT is defined as a biological process in which injured TECs undergo phenotypic transformation into myofibroblasts with the consequent production of ECM and various pro-fibrotic molecules, which is regarded as an integral part of interstitial fibrosis.[5] Although, based on evidence, complete EMT of TECs is not a major contributor to interstitial myofibroblasts in kidney fibrosis, partial EMT, where damaged TECs remain associated with their basement membrane and co-express both epithelial and mesenchymal markers, is an indispensable stage for fibrogenesis in the interstitium.[2,6,7] Preventing the acquisition of an EMT program in injured TECs results in restoration of functional TECs, inhibition of the pathological secretome, and alleviation of cell-cycle arrest, thereby facilitating the repair and regeneration of the fibrotic kidney.[8,9]

SNAI1 is a key transcription factor that activates the EMT program during embryonic development, fibrogenesis, and tumor progression by regulating the expression of multiple pro-fibrotic genes.[10,11] In mouse models of experimentally induced renal fibrosis, conditional deletion of Snail1 in proximal TECs resulted in inhibition of the EMT program, maintenance of TEC integrity, restoration of cell proliferation, dedifferentiation-associated repair and regeneration of the kidney parenchyma, and attenuation of interstitial fibrosis.[7] Snail1-induced fibrosis can be reversed *in vivo*, and obstructive nephropathy can be therapeutically ameliorated in mice by targeting Snail1 expression.[6] These results confirm the vital role of Snail1 in the progression of renal fibrosis. Glycogen synthase kinase-3β (GSK-3β) binds to and phosphorylates Snail1 at two Ser-rich motifs to regulate the transcriptional activity and function of this protein.[12] Together with Snail1, GSK-3β function is considered a molecular switch that triggers an EMT program. Several pathways increase Snail1 activity by influencing GSK3β-mediated phosphorylation including Wnt/β-catenin, PI3K/AKT, ERK, nuclear factor-κB (NF-κB), and Notch signaling.[13–16] Therefore, the GSK3β/Snail axis plays an important role in renal fibrogenesis.

Minichromosome maintenance 6 (MCM6) belongs to the MCM protein family, which forms the catalytic core of eukaryotic replicative helicase.[17] Existing evidence indicated that MCM plays an important role in DNA replication and DNA damage repair.[18] Recently, MCM is considered a potential marker of cell proliferation, especially in malignant cells, and is associated with the progression and prognosis of malignant tumors.[19] MCM6 has been identified as a driver of S/G2 cell-cycle progression and a potential diagnostic and prognostic marker

[1]Department of Nephrology, Union Hospital, Tongji Medical College, Huazhong University of Science and Technology, Wuhan 430022, China
[2]Lead contact
*Correspondence: drzhangchun@hust.edu.cn
https://doi.org/10.1016/j.isci.2023.107940

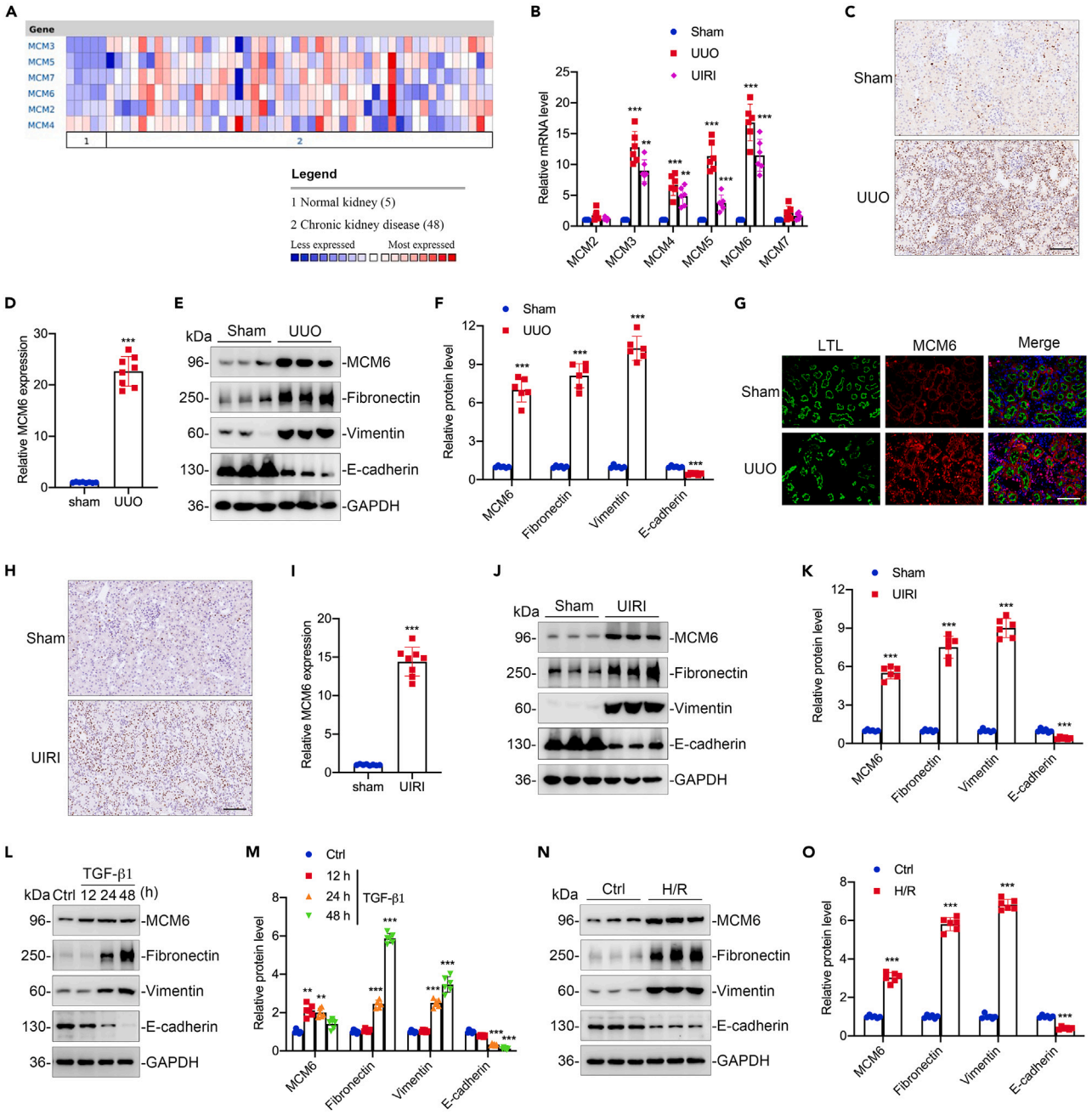

Figure 1. Minichromosome maintenance 6 (MCM6) increases in proximal tubular epithelial cells during renal fibrogenesis

(A) Graphical representation showing the relative expression patterns of MCM2-7 in chronic kidney disease (CKD). The data are obtained from the Nephroseq website.

(B) Graphical representation showing the mRNA level of MCM2-7 in the fibrotic kidney of unilateral ureteral obstruction (UUO) and unilateral ischemia reperfusion injury (UIRI) mice models. n = 6 mice per group.

(C and D) Immunohistochemical staining and summarized data showing the expression of MCM6 in UUO models. Scale bar, 50 μm.

(E and F) Representative western blots and summarized data showing the renal expression of MCM6, fibronectin, vimentin, and E-cadherin in UUO mice. n = 6 mice per group.

(G) Colocalization staining of MCM6 (red) and lotus tetragonolobus lectin (LTL, green) in the kidneys of UUO model mice. LTL, a proximal tubule marker. Scale bar, 25 μm.

(H and I) Immunohistochemical staining and summarized data showing the expression of MCM6 in UIRI models. Scale bar, 50 μm.

(J and K) Representative western blots and summarized data showing the renal expression of MCM6, fibronectin, vimentin, and E-cadherin in UIRI mice. n = 6 mice per group.

Figure 1. *Continued*

(L and M) Representative western blots and summarized data showing the expression of MCM6, fibronectin, vimentin, and E-cadherin in transforming growth factor (TGF)-β1-treated proximal tubular epithelial cells (TECs). n = 6.

(N and O) Representative western blots and summarized data showing the expression of MCM6, fibronectin, vimentin, and E-cadherin in TECs with hypoxia-reoxygenation (H/R) treatment. n = 6. **p < 0.01, ***p < 0.001 versus sham group or Ctrl group. All data are graphed as mean ± SEM. See also Figure S1.

in hepatocellular carcinoma (HCC).[20] And it was reported that MCM6 promotes EMT by regulating MEK/ERK signaling in HCC.[21] Moreover, the serum MCM6 level is a promising independent biomarker to detect preclinical early recurrence of HCC, especially in alpha-fetoprotein-negative patients with small HCC.[22] Although many studies have clarified the significance of MCM6 in a variety of malignancies, its role in kidney disease is poorly understood. Recently, MCM6 was involved in karyomegalic interstitial nephritis by regulating cell-cycle activity.[23] However, owing to the limited studies on MCM6-deficient animal models, the biological function of MCM6 in renal pathology is largely unknown.

In the present study, we identified for the first time that tubular injury triggered the upregulation of MCM6 in proximal TECs and evaluated the kidney protective role of MCM6 in renal fibrogenesis, which is associated with the activation of ERK/GSK-3β/Snail1 signaling. In addition, our findings revealed the downregulation of DUSP6 in the fibrotic kidneys and the potential role of DUSP6 in regulating ERK activity. In summary, endogenous MCM6 level was of great importance for maintaining tubular epithelial integrity and TECs function, and it could be a potential target for antifibrotic therapeutic strategies in patients with CKD.

RESULTS

Elevated expression of MCM6 in fibrotic kidneys and cultured TECs

To determine the expression pattern of MCMs proteins in the kidney during renal fibrogenesis, we first examined the expression of the MCMs in patients with CKD using the Nephroseq website (Mendeley Data: http://nephroseq.org). We found that the expression of MCM3, MCM5, MCM6, and MCM7 was higher in patients with CKD (Figure 1A). To confirm the role of the MCM family in the pathogenesis of CKD, two unrelated *in vivo* fibrotic models—UUO and UIRI—were used to establish chronic kidney fibrosis models. We examined the mRNA level of the MCM family in fibrotic kidneys using qRT-PCR and found that the level of MCM6 was most significantly upregulated in both fibrotic models (Figure 1B; prime sequences were seen in Table 1). Therefore, we choose MCM6 for further analysis. Compared with that in normal kidney tissues, MCM6 was markedly increased in the tubulointerstitial area in UUO mice as observed in the immunohistochemistry results (Figures 1C and 1D), which was further demonstrated by immunoblotting assay, accompanied by the upregulation of fibronectin and vimentin levels (Figures 1E and 1F). To confirm the renal localization of MCM6, we dually stained cortex sections for MCM6 and Lotus tetragonolobus lectin (LTL, a proximal tubular marker) and showed that LTL-positive proximal tubular cells (green) were co-localized with MCM6 (red), suggesting that the increase in MCM6 mainly occurred in proximal TECs after obstruction injury (Figure 1G). Consistently, MCM6 was also significantly increased in UIRI-induced renal fibrosis, as determined through immunohistochemistry (Figures 1H and 1I) and immunoblotting analyses (Figures 1J and 1K). In addition, to determine whether the upregulation of MCM6 was secondary to tubular epithelial injury, we treated proximal TECs (NRK-52E) with transforming growth factor β1 (TGF-β1) or H/R stimulation. After TGF-β1 treatment for 12 h, we found that MCM6 expression began to increase significantly in NRK-52E cells as well as in HK-2 cells (Figure S1), which preceded the changes of fibronectin, vimentin, and E-cadherin—the three classic markers of tubular EMT (Figures 1L and 1M). And the upregulation of MCM6 was also observed in NRK-52E cells in response to H/R stimulation (Figures 1N and 1O). In summary, these results indicate that renal fibrosis is associated with an increase in MCM6 expression in the tubulointerstitial area, particularly in proximal TECs.

MCM6 deficiency promotes partial EMT program in TECs

To explore the possible role of MCM6 in renal fibrosis, small interfering RNA (siRNA) targeting MCM6 (si-MCM6) were transfected into NRK-52E cells to disrupt MCM6 expression, and the inhibitory efficiency of MCM6 level was determined by immunoblotting (Figures 2A and 2B) and qRT-PCR analyses (Figure 2C). TGF-β1 is a critical mediator implicated in renal TIF; therefore, we evaluated whether MCM6 expression had an effect on the partial EMT process in TGF-β1-treated TECs. As shown in Figure 2D, TECs exhibited the loss of cell–cell contacts and their typical epithelial cell morphology and acquired the elongated spindle-shaped mesenchymal phenotype after incubation with TGF-β1 for 48 h, and MCM6 deficiency aggravated these morphological changes in TECs. Simultaneously, partial EMT induction was confirmed through the loss of E-cadherin and the accumulation of fibronectin, α-SMA, and vimentin in response to TGF-β1 stimulation, whereas silencing of MCM6 further promoted the tubular EMT process (Figures 2E–2G). And immunofluorescence data further revealed the disruption of E-cadherin and the accumulation of fibronectin induced by MCM6 knockdown (Figure 2H). Consistent with TGF-β1-induced profibrotic changes, MCM6 deficiency aggravated H/R-induced levels of fibronectin, α-SMA, and vimentin, accompanied by the loss of E-cadherin (Figures 2I–2K; prime sequences were seen in Table 1). These results indicate that MCM6 is involved in the tubular partial EMT process, ECM deposition, and myofibroblast activation during the progression of renal fibrosis.

In vivo knockdown of MCM6 aggravates UUO-induced renal fibrosis

To further investigate the role of MCM6 in renal fibrogenesis, AAV harboring MCM6 (AAV-sh-MCM6) was delivered into mouse kidneys via intraparenchymal injection to knock down the expression of MCM6 in renal tubules before establishing the UUO model (Figure 3A). Renal expression of MCM6 was robustly blocked in UUO-induced mice that received AAV-sh-MCM6 as evidenced by the results of

Table 1. Prime sequences used in qRT-PCR

Gene	Species	Sequence
MCM2	Mouse	Forward: GTCAGCTCTATCTCGTCCCC Reverse: ATCAGAACTACCAACGTATCCGC
MCM3	Mouse	Forward: AGCGCAGAGAGACTACTTGGA Reverse: GCGGTTAGCCCTCTTTTCATTC
MCM4	Mouse	Forward: TTTGTGCGCGTTTGCAACTA Reverse: GTGACGACCTGCTTTCCTCA
MCM5	Mouse	Forward: TCTAGGAGGGCTGAGGTACAG Reverse: ACTCCTTGAATCGCCTCTGC
MCM6	Mouse	Forward: GAATCATTGGGGAGCGGTCA Reverse: GACACCACAAAAAGCCCACC
MCM7	Mouse	Forward: TCGGAGATAGCTGCAGTAGAAA Reverse: TTGAGTCGACCAACTCAGGGT
DUSP5	Mouse	Forward: AGCGTGGTCTCTCCCAACTT Reverse: GGTACGGAATGTGCAGTAGGT
DUSP6	Mouse	Forward: ATAGATACGCTCAGACCCGTG Reverse: ATCAGCAGAAGCCGTTCGTT
GAPDH	Mouse	Forward: TGGCCTTCCGTGTTCCTAC Reverse: GAGTTGCTGTTGAAGTCGCA
MCM6	Rattus	Forward: CGATGCTTGGGGACAGTTGA Reverse: CAGGACAAGCACAAAGTGCC
Fibronectin	Rattus	Forward: CCCTTCCACACCCCAATCTT Reverse: ACTGGGTTGTTGGTGGGATG
Vimentin	Rattus	Forward: GCAGCCTCTATTCCTCGTCC Reverse: GAAGCGGTCATTCAGCTCCT
α-SMA	Rattus	Forward: TTGTCCACCGCAAATGCTTC Reverse: TGAAGGCGCTGATCCACAAA
GAPDH	Rattus	Forward: GCATCTTCTTGTGCAGTGCC Reverse: TACGGCCAAATCCGTTCACA

immunohistochemistry and immunoblotting analyses. Notably, hematoxylin-eosin (HE) and Masson's trichrome staining showed that delivery of AAV-sh-MCM6 resulted in more significant tubular injury and fibrotic lesions than that induced by the delivery of negative-control AAV (AAV-sh-Ctrl) (Figures 3B–3D). And examination of fibrotic markers showed that knockdown of MCM6 expression further aggravated the accumulation of fibronectin, vimentin, and α-SMA in the obstructed kidneys, accompanied with the loss of E-cadherin (Figures 3B–3G). Furthermore, α-SMA-positive myofibroblasts and fibronectin accumulation were greatly increased in the interstitium of the obstructed kidney in AAV-sh-MCM6 group mice compared with that in the AAV-sh-Ctrl group mice by immunofluorescence staining (Figure 3H). These data suggest that MCM6 deficiency exacerbated UUO-induced renal fibrosis.

In vivo knockdown of MCM6 exacerbates UIRI-induced renal fibrosis

To further confirm the role of MCM6 in renal fibrosis, AAV-sh-MCM6 virions were delivered into mouse kidneys before establishing the UIRI model (Figure 4A). As shown in Figures 4B–4E, the injured kidney displayed typical features of renal fibrosis after UIRI, whereas knockdown of MCM6 expression further aggravated tubular damage and atrophy, the severity of TIF, and the area of interstitial fibrosis. When examining the mesenchymal markers, we found that MCM6 ablation remarkably contributed to the accumulation of fibronectin, α-SMA, and vimentin in the tubulointerstitial area as observed by immunostaining (Figures 4B–4E). And the changes in these fibrosis markers were further validated by immunoblotting (Figures 4F and 4G) and immunofluorescence data (Figure 4H). These results showed that MCM6 deficiency accentuated renal fibrosis in UIRI mice, which was consistent with the results observed in UUO mice, suggesting the significance of MCM6 in renal fibrogenesis.

In vivo overexpression of MCM6 alleviates UUO-induced renal fibrosis

To clarify the therapeutic efficacy of targeting MCM6 in the progression of renal fibrosis, AAV harboring MCM6 (AAV-OE-MCM6) was delivered into mouse kidneys via intraparenchymal injection to overexpress MCM6 in renal tubules before establishing the UUO model (Figure 5A). Immunohistochemistry and immunoblotting analyses showed that kidney MCM6 expression greatly increased in the mice with

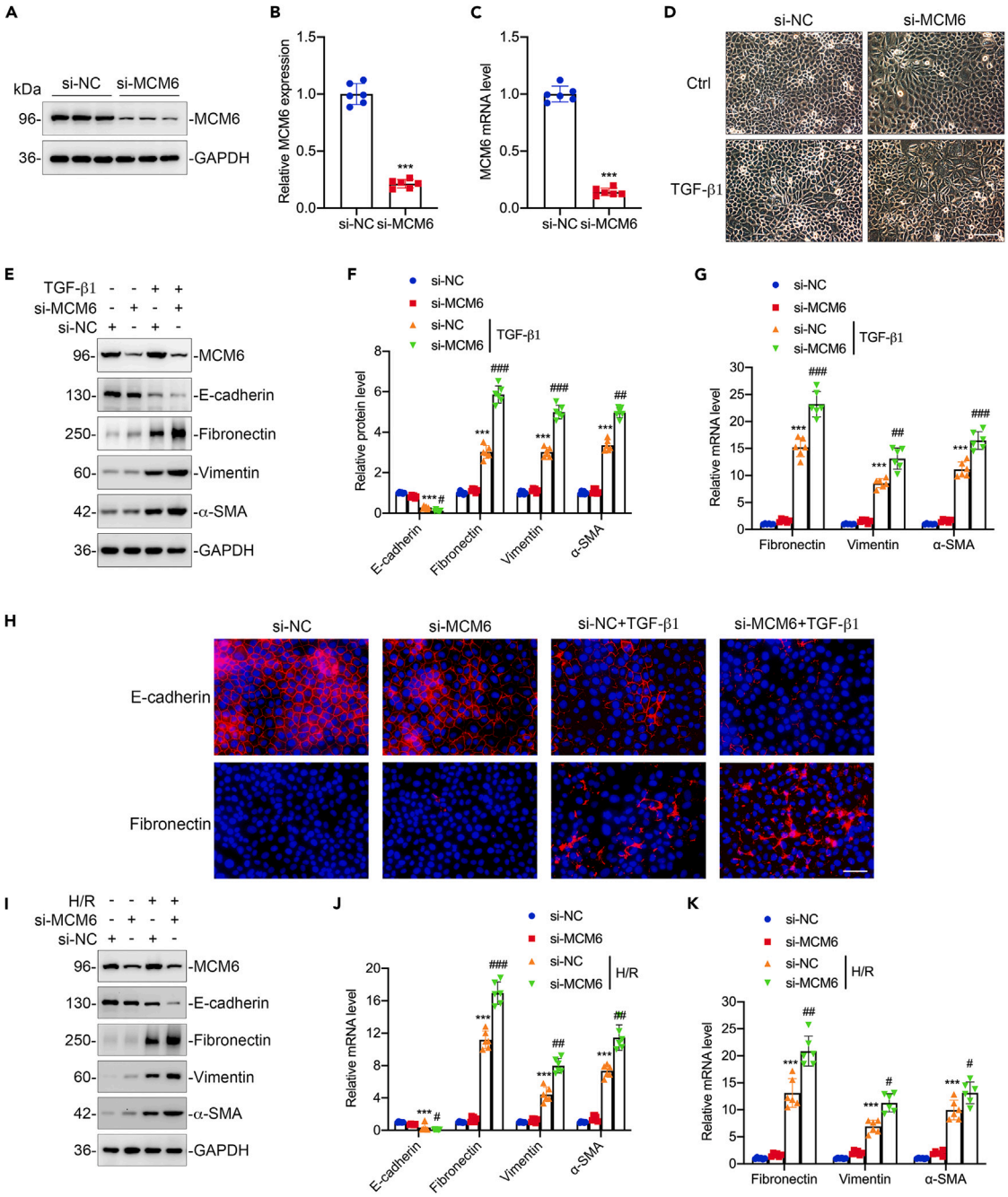

Figure 2. MCM6 deficiency aggravated tubular partial epithelial–mesenchymal transition in TGF-β1-induced TECs

(A and B) Representative western blots and summarized data of MCM6 expression in TECs transfected with small interfering RNA (siRNA)-targeted MCM6 (si-MCM6). n = 6.

(C) Graphical representation showing the mRNA level of MCM6 in TECs transfected with si-MCM6. n = 6.

(D) Representative images of the polarized morphology of TECs in different groups. Cells were transfected with si-MCM6 or si-NC and treated with TGF-β1 for 48 h. n = 6. Scale bar, 50 μm.

(E and F) Representative western blots and summarized data showing the expression of MCM6, E-cadherin, fibronectin, α-SMA, and vimentin in four groups, as indicated. n = 6.

(G) Graphical representation showing the mRNA levels of fibronectin, α-SMA, and vimentin in different groups. n = 6.

(H) Representative micrographs showing the immunofluorescence staining images of fibronectin and α-SMA in four groups, as indicated. Scale bar, 50 μm.

Figure 2. *Continued*

(I and J) Representative western blots and summarized data showing the expression of MCM6, E-cadherin, fibronectin, α-SMA, and vimentin in four groups, as indicated. Cells were transfected with si-MCM6 or si-NC and then treated with H/R stimulation for 48 h. n = 6.

(K) Graphical representation showing the mRNA levels of fibronectin, α-SMA, and vimentin in four groups, as indicated. n = 6. $^{**}p < 0.01$, $^{***}p < 0.001$ versus si-NC group. $^{\#}p < 0.05$, $^{\#\#}p < 0.01$, $^{\#\#\#}p < 0.001$ versus si-NC + TGF-β1 or si-NC + H/R group. All data are graphed as mean ± SEM. See also Figure S2.

AAV-OE-MCM6 delivery. Notably, the obstructed kidneys displayed typical features of renal fibrosis following UUO, and overexpression of MCM6 significantly decreased the severity of TIF and the area of interstitial fibrosis (Figures 5B–5D). Immunostaining and immunoblotting data showed that the increased levels of fibronectin, vimentin, and α-SMA were prominently attenuated in UUO-induced mice, particularly in the tubulointerstitial area, after AAV-OE-MCM6 delivery (Figures 5B–5G). Moreover, overexpression of MCM6 distinctly inhibited the loss of E-cadherin, indicating that tubular MCM6 level maintains the integrity of epithelial cells (Figures 5F and 5G). Immunofluorescence data further revealed that α-SMA-positive myofibroblasts and fibronectin accumulation were dramatically decreased in the AAV-OE-MCM6 group mice compared with that in the negative-control group mice (Figure 5H). These data further confirmed the essential role of MCM6 such as maintaining epithelial integrity and tubular function, protecting against tubular injury or dedifferentiation, and eventually involving in fibrogenesis.

Overexpression of MCM6 suppresses renal fibrosis in UIRI mice

To further examine the functional role MCM6 in renal fibrosis, AAV-OE-MCM6 virions were delivered into mouse kidneys to overexpress MCM6 before establishing the UIRI model (Figure 6A). As shown in Figures 6B–6D, compared with that in the negative control mice, the extent of UIRI-induced tubular damage and interstitial area was substantially alleviated after the delivery of AAV-OE-MCM6. And UIRI-induced accumulation of fibronectin, vimentin, and α-SMA was reversed by MCM6 overexpression, accompanied by the restoration of E-cadherin expression (Figures 6B–6G). Moreover, immunofluorescence data showed the decreased level of α-SMA-positive myofibroblasts and fibronectin deposition in UIRI mice after the delivery of AAV-OE-MCM6 (Figure 6H), which was consistent with the results observed in the UUO model mice. These results further exhibited a potent effect of MCM6 on attenuating fibrotic response in renal fibrogenesis.

MCM6 modulates the activation of ERK/GSK-3β/Snail1 signaling pathway in tubular partial EMT progress

Snail1—a prominent inducer of EMT—is a highly labile protein and a critical transcriptional regulator of E-cadherin that represses epithelial-related gene expression and contributes to the mesenchymal phenotype.[16] To explore the potential cellular signaling pathways, we examined GSK-3β-mediated Snail activity and ERK pathway upon MCM6 dysregulation conditions, which are known to play pivotal roles in tubular EMT progress and the progression of kidney fibrosis. As shown in Figures 7A–7D, compared with that in the sham group, the upregulation of phospho-ERK, phospho-GSK-3β, and Snail1 were observed in UUO mice, and these increases were further elevated in the kidneys of UUO mice following the delivery of AAV-sh-MCM6; however, these increases were markedly inhibited in the kidneys of UUO mice that were delivered AAV-OE-MCM6. In addition, *in vitro* studies showed that the induction of phospho-ERK and phospho-GSK-3β were observed in NRK-52E cells treated with TGF-β1 for 1 h, and the expression of Snail1 was increased in TGF-β1-treated NRK-52E cells for 48 h. MCM6 deficiency further aggravated the increase in phospho-ERK, phospho-GSK-3β, and Snail1 expression in TECs upon TGF-β1 stimulation (Figures 7E–7H). These studies indicate a potential role of MCM6 in the regulation of ERK/GSK-3β/Snail1 signaling. To validate the involvement of ERK/GSK-3β/Snail1 signaling in MCM6-induced renal fibrosis, a MEK1/2 inhibitor U0126 and a GSK-3β inhibitor SB216763 were used alone or combined to block ERK signaling and GSK-3beta activity in NRK-52E cells. As shown in Figures 7I–7K, pretreatment with U0126 blocked the upregulation of phospho-ERK, phospho-GSK-3β, and Snail1 levels, pretreatment with SB216763 suppressed the increase in phospho-GSK-3β and Snail1 levels, and co-pretreatment with U0126 and SB216763 further inhibited the expression of Snail1, in MCM6-deficient NRK-52E cells. Collectively, our data demonstrate that MCM6 protects against renal fibrosis by regulating ERK/GSK-3β/Snail1 signaling.

DUSP6 is downregulated in renal fibrosis and associates with the activation of ERK signaling in MCM6-mediated partial EMT progress

Dual-specificity phosphatases (DUSPs), which belong to the family of protein tyrosine phosphatases, are expressed in various types of kidney cells at different levels and have been implicated in various kidney diseases.[24] The expression of DUSPs can be divided into four groups according to their basic expression level in the kidney; DUSP5 and DUSP6 are negative regulators of ERK signaling and belong to the low and moderate expression groups, respectively.[25] Based on data from the website of Nephroseq, we found that the expression of DUSP5 and DUSP6 (especially that of DUSP6) was notably decreased in various types of human CKD including immunoglobulin A (IgA) nephropathy, focal segmental glomerulosclerosis, membranous glomerulonephropathy, minimal change disease, and thin basement membrane disease (Figure 8A). To clarify the expression of DUSP5 and DUSP6 in CKD, we examined their mRNA levels in fibrotic kidneys using qRT-PCR and found that compared with that of DUSP5, the mRNA level of DUSP6 was more significantly downregulated in kidney from UUO and UIRI mice (Figure 8B). Therefore, we mainly discussed the role of DUSP6 in renal fibrosis and whether its expression is mediated by MCM6. As shown in Figures 8C and 8D, compared with that in normal kidney tissues, DUSP6 expression was dramatically decreased in fibrotic kidneys of mice with UUO and UIRI. And immunostaining data further confirmed this result (Figures 8E and 8F). Moreover, TGF-β1 and H/R treatment led to a significant decrease in DUSP6 expression in TECs (Figures 8G and 8H), suggesting a potential role for DUSP6 in renal fibrogenesis. To corroborate the potential role of DUSP6 in ERK/GSK-3β/Snail1 signaling, MCM6 overexpress plasmid was transfected into NRK-52E cells

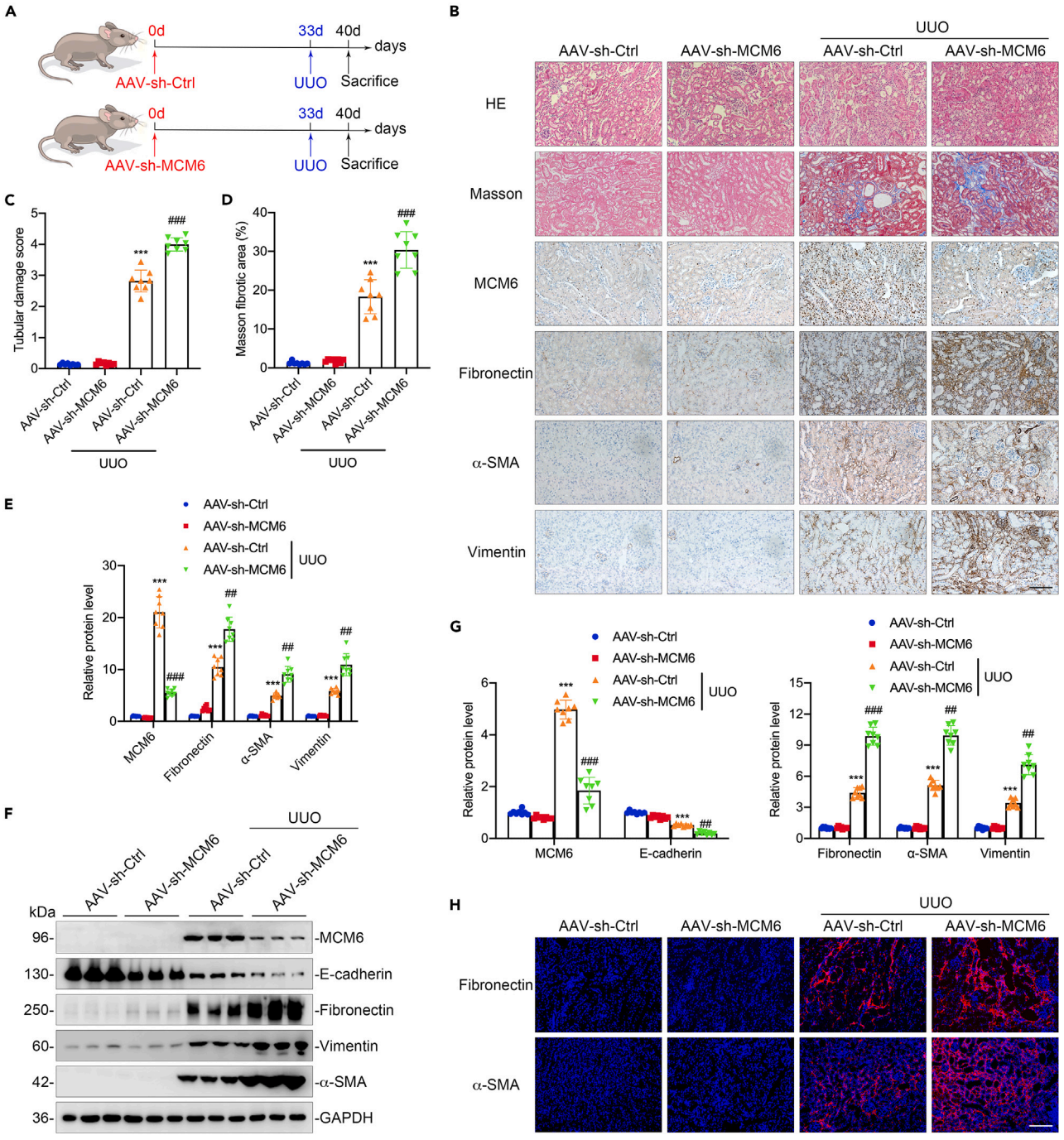

Figure 3. Knockdown of MCM6 aggravated UUO-induced renal fibrosis

(A) Experimental design. Red arrows show the delivery of AAV-sh-Ctrl or AAV-sh-MCM6 into mouse kidney through intraparenchymal injection. Blue arrows show the time of renal UUO surgery.

(B) Representative micrographs showing hematoxylin and eosin (H&E) staining; Masson's trichrome staining; and immunostaining of MCM6, fibronectin, α-SMA, and vimentin in four groups, as indicated. Scale bar, 50 μm.

(C–E) Graphical representations showing the tubular damage score; fibrotic area; and the expression of MCM6, fibronectin, α-SMA, and vimentin in four groups, as indicated.

(F and G) Representative western blots and summarized data showing the expression of MCM6, E-cadherin, fibronectin, α-SMA, and vimentin in four groups, as indicated. n = 8 mice per group.

(H) Representative micrographs showing the immunofluorescence staining of fibronectin and α-SMA in four groups, as indicated. Scale bar, 50 μm. ***$p < 0.001$ versus AAV-sh-Ctrl group. $^{\#\#}p < 0.01$, $^{\#\#\#}p < 0.001$ versus AAV-sh-Ctrl + UUO group. All data are graphed as mean ± SEM.

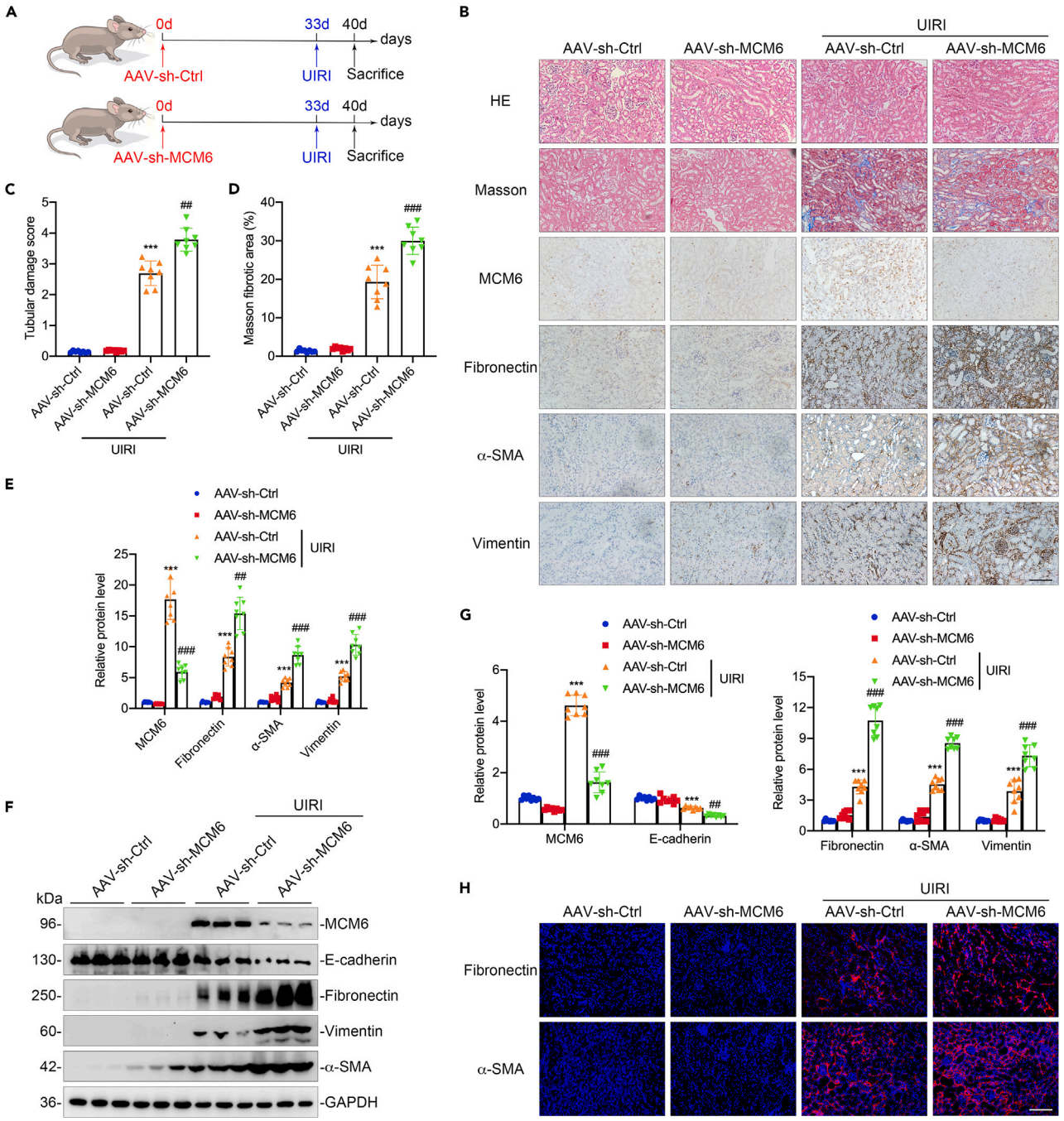

Figure 4. Blockade of MCM6 aggravated UIRI-induced renal fibrosis

(A) Experimental design. Red arrows show the delivery of AAV-sh-Ctrl or AAV-sh-MCM6 into mouse kidney through intraparenchymal injection. Blue arrows show the time of renal UIRI surgery.

(B) Representative micrographs showing H&E staining; Masson's trichrome staining; and immunostaining of MCM6, fibronectin, α-SMA, and vimentin in four groups, as indicated. Scale bar, 50 μm.

(C–E) Graphical representation showing the tubular damage score; fibrotic area; and the expression of MCM6, fibronectin, α-SMA, and vimentin in four groups, as indicated.

(F and G) Representative western blots and summarized data showing the expression of MCM6, E-cadherin, fibronectin, α-SMA, and vimentin in four groups, as indicated. n = 8 mice per group.

(H) Representative micrographs showing the immunofluorescence staining images of fibronectin and α-SMA in four groups, as indicated. Scale bar, 50 μm. ***$p < 0.001$ versus AAV-sh-Ctrl group. $^{\#\#}p < 0.01$, $^{\#\#\#}p < 0.001$ versus AAV-sh-Ctrl + UIRI group. All data are graphed as mean ± SEM. See also Figure S3.

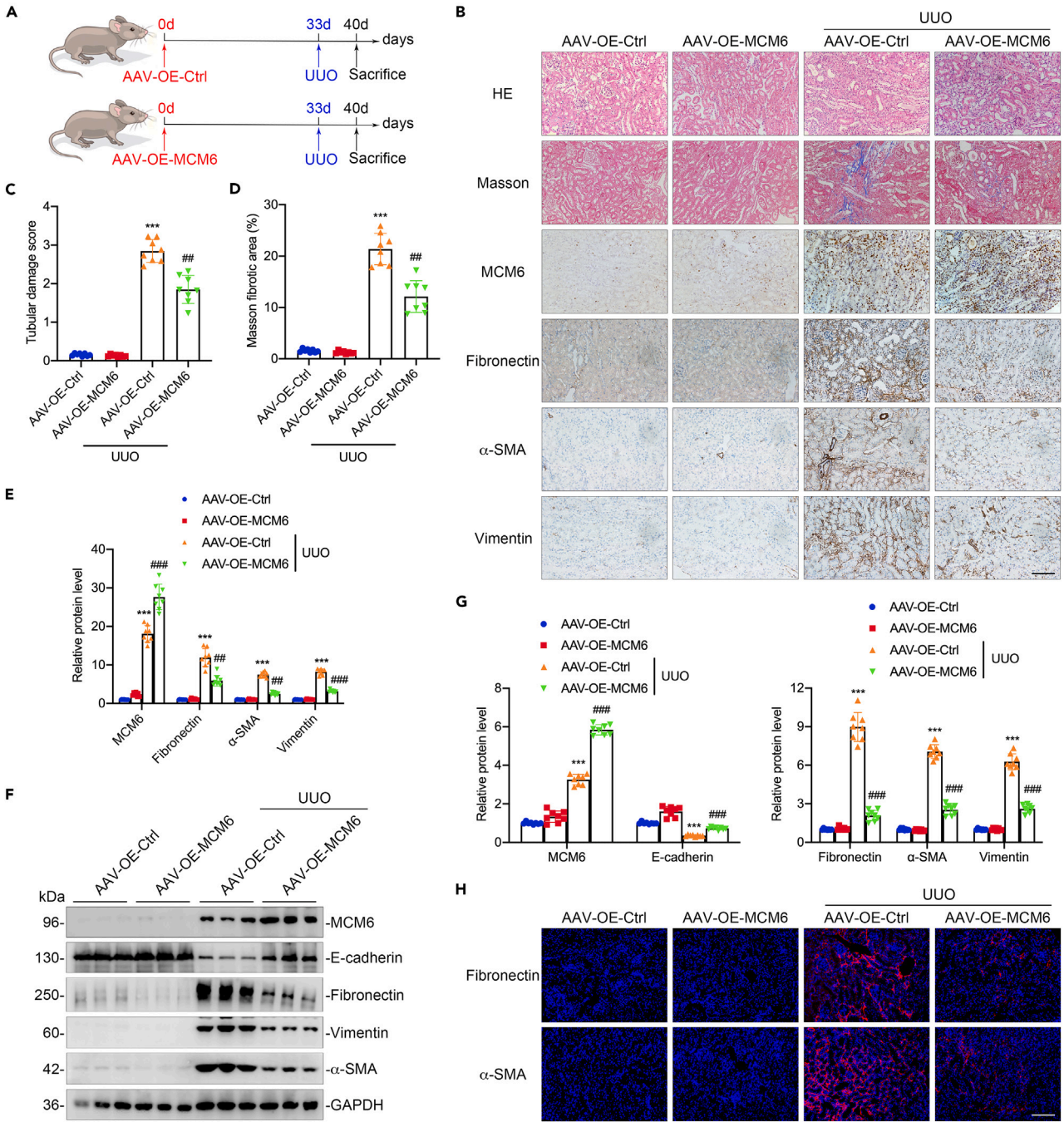

Figure 5. Overexpression of MCM6 attenuated UUO-induced renal fibrosis

(A) Experimental design. Red arrows show the delivery of AAV-OE-Ctrl or AAV-OE-MCM6 into mouse kidney through intraparenchymal injection. Blue arrows show the time of renal UUO surgery.

(B) Representative micrographs showing H&E staining; Masson's trichrome staining; and immunostaining of MCM6, fibronectin, α-SMA, and vimentin in four groups, as indicated. Scale bar, 50 μm.

(C–E) Graphical representations showing the tubular damage score; fibrotic area; and the expression of MCM6, fibronectin, α-SMA, and vimentin in four groups, as indicated.

(F and G) Representative western blots and summarized data showing the expression of MCM6, E-cadherin, fibronectin, α-SMA, and vimentin in four groups, as indicated. n8 mice per group.

(H) Representative micrographs showing the immunofluorescence staining of fibronectin and α-SMA in four groups, as indicated. Scale bar, 50 μm. ***$p < 0.001$ versus AAV-OE-Ctrl group. $^{\#\#}p < 0.01$, $^{\#\#\#}p < 0.001$ versus AAV-OE-Ctrl + UUO group. All data are graphed as mean ± SEM.

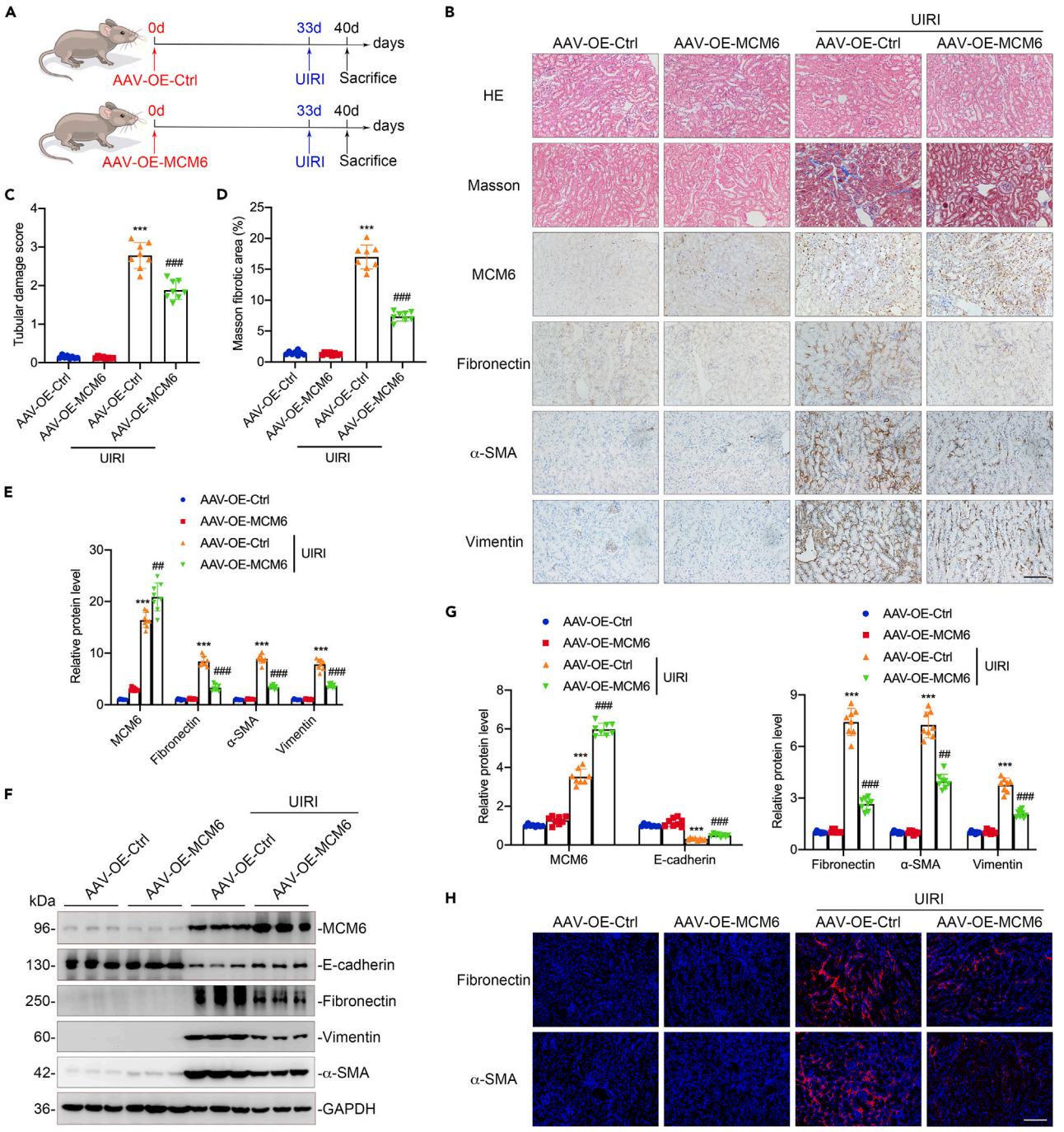

Figure 6. Overexpression of MCM6 ameliorated UIRI-induced renal fibrosis

(A) Experimental design. Red arrows show the delivery of AAV-OE-Ctrl or AAV-OE-MCM6 into mouse kidney through intraparenchymal injection. Blue arrows show the time of renal UIRI surgery.

(B) Representative micrographs showing H&E staining; Masson's trichrome staining; and immunostaining of MCM6, fibronectin, α-SMA, and vimentin in four groups, as indicated. Scale bar, 50 μm.

(C–E) Graphical representations showing the tubular damage score; fibrotic area; and the expression of MCM6, fibronectin, α-SMA, and vimentin in four groups, as indicated.

(F and G) Representative western blots and summarized data showing the expression of MCM6, E-cadherin, fibronectin, α-SMA, and vimentin in four groups, as indicated. n = 8 mice per group.

(H) Representative micrographs showing the immunofluorescence staining images of fibronectin and α-SMA in four groups, as indicated. Scale bar, 50 μm. ***$p < 0.001$ versus AAV-OE-Ctrl group. $^{\#\#}p < 0.01$, $^{\#\#\#}p < 0.001$ versus AAV-OE-Ctrl + UIRI group. All data are graphed as mean ± SEM. See also Figure S3.

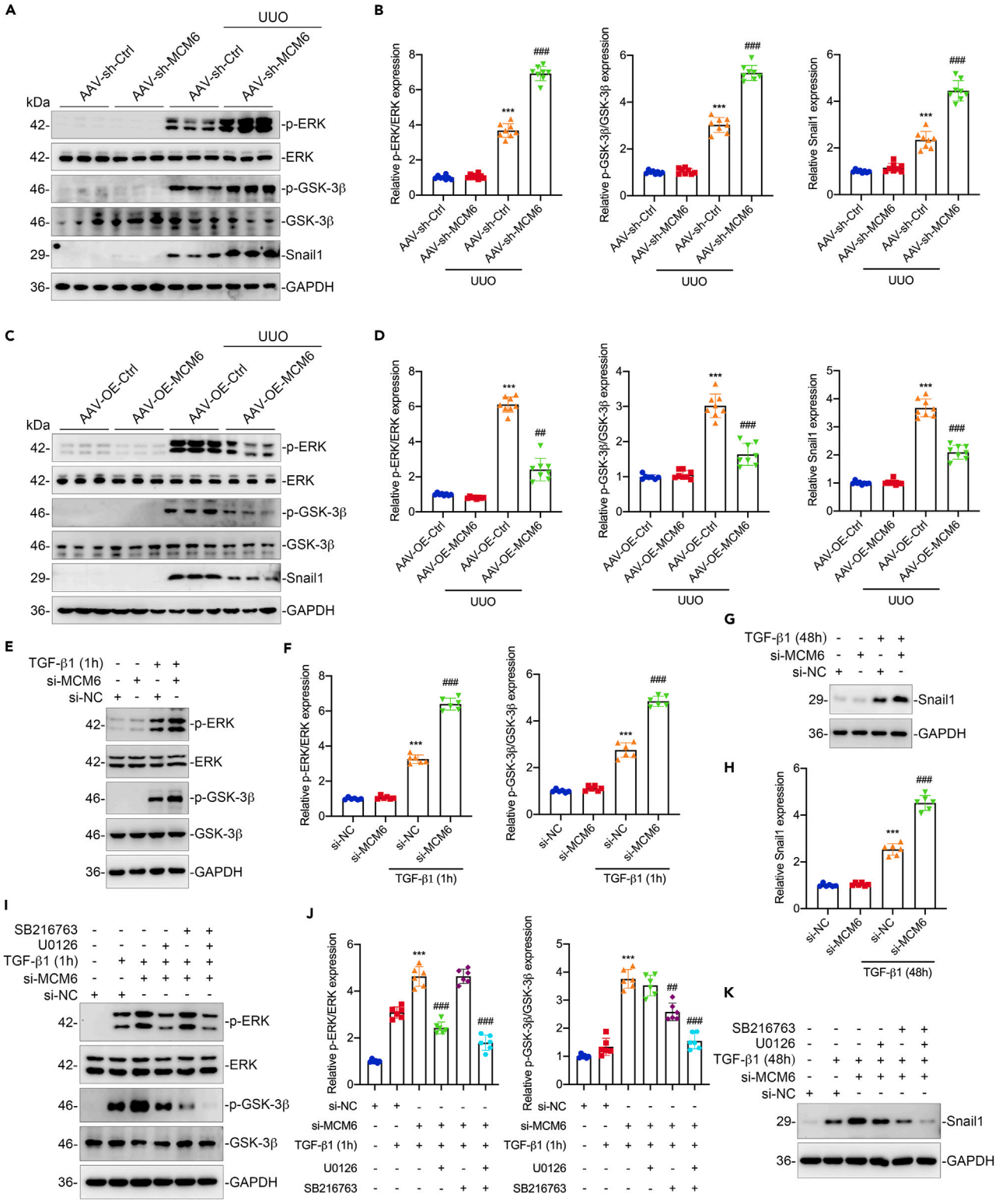

Figure 7. ERK/GSK-3β/Snail1 signaling was activated in MCM6-induced renal fibrosis

(A and B) Representative western blots and summarized data showing the expression of ERK, phospho-ERK, GSK-3β, phospho-GSK-3β, and Snail1 in four groups, as indicated. n = 8 mice per group. ***p < 0.001 versus AAV-sh-Ctrl, $^{###}$p < 0.001 versus AAV-sh-Ctrl + UUO.

Figure 7. *Continued*

(C and D) Representative western blots and summarized data showing the expression of ERK, phospho-ERK, GSK-3β, phospho-GSK-3β, and Snail1 in four groups, as indicated. n = 8 mice per group. ***p < 0.001 versus AAV-OE-Ctrl, ##p < 0.01, ###p < 0.001 versus AAV-OE-Ctrl + UUO. (E and F) Representative western blots and summarized data showing the expression of ERK, phospho-ERK, GSK-3β, and phospho-GSK-3β in four groups, as indicated. TECs were transfected with si-NC or si-MCM6 for 48 h and treated with TGF-β1 for 1 h. n = 6. ***p < 0.001 versus si-NC, ###p < 0.001 versus si-NC + TGF-β1 (1 h).

(G and H) Representative western blots and summarized data showing the expression of Snail1 in four groups, as indicated. TECs were transfected with si-NC or si-MCM6 and treated with TGF-β1 for 48 h. n = 6. ***p < 0.001 versus si-NC, ###p < 0.001 versus si-NC + TGF-β1 (48 h).

(I and J) Representative western blots and summarized data showing the expression of ERK, phospho-ERK, GSK-3β, and phospho-GSK-3β in six groups, as indicated. TECs were transfected with si-NC or si-MCM6 for 48 h, pretreated with U0126 (30 μM) or SB216763 (50 μM) for 1 h, and then treated with TGF-β1 for 1 h. n = 6. ***p < 0.001 versus si-NC, ##p < 0.01, ###p < 0.001 versus si-NC + TGF-β1 (1 h).

(K) Representative western blots showing the expression of Snail1 in six groups, as indicated. TECs were transfected with si-NC or si-MCM6, pretreated with U0126 (30 μM) or SB216763 (50 μM) for 1 h, and then treated with TGF-β1 for 48 h. n = 6. All data are graphed as mean ± SEM.

to induce MCM6 expression, and the overexpression efficiency of MCM6 level was determined by immunoblotting (Figure 8I). TGF-β1-induced upregulation of phospho-ERK, phospho-GSK-3β, and Snail1 levels were remarkedly inhibited by DUSP6 overexpression, indicating that DUSP6 negatively regulates the activation of ERK/GSK-3β/Snail1 signaling (Figures 8I and 8J). Given the role of MCM6 in the regulation of ERK/GSK-3β/Snail1 signaling, we suspected whether MCM6 participates in the regulation of DUSP6 expression. To validate our hypothesis, we detected the expression of DUSP6 in fibrotic kidneys with MCM6 deficiency or MCM6 overexpression. And we found that DUSP6 expression was further decreased in the kidneys of UUO mice injected with AAV-sh-MCM6; however, this decrease was significantly reversed in the kidneys of UUO mice injected with AAV-OE-MCM6, suggesting that MCM6 positively regulates DUSP6 expression (Figures 8K–8N). In summary, our results reveal the dysregulation of endogenous DUSP6 levels in kidney fibrosis and suggest a potential role of DUSP6 in the regulation of ERK/GSK-3β/Snail1 signaling. Moreover, the functional role of DUSP6 in renal fibrosis is partially mediated by MCM6.

DISCUSSION

Despite its implications in the progression of various malignant tumors, the exact physiological function of MCM6 in kidney diseases remains unclear.[26] Little is known about the functional contributions and prognostic value of MCM6 in renal fibrosis. In this study, we identified for the first time that MCM6 was significantly upregulated in fibrotic kidneys of UUO or UIRI mouse models and cultured TECs in response to TGF-β1 or H/R stimulation. Knockdown of MCM6 expression, both *in vivo* and *in vitro*, further aggravated tubular partial EMT progression, ECM accumulation, and myofibroblast activation in UUO and UIRI mice. Whereas overexpression of MCM6 substantially inhibited the deposition of these fibrotic markers and restored the expression of E-cadherin, indicating that MCM6 plays a critical role in maintaining epithelial integrity and tubular function, eventually retarding renal fibrogenesis. In addition, we further evaluated the potential role of DUSP6 (a negative regulator of the ERK pathway) in the regulation of ERK/GSK-3β/Snail1 signaling. And the involvement of DUSP6-mediated ERK/GSK-3β/Snail1 signaling in renal fibrosis was partially regulated by MCM6 expression. In summary, our studies provide direct evidence for the important role of MCM6 in maintaining the tubular epithelial phenotype and protecting against renal fibrosis, indicating the significance of preserving basal MCM6 levels in fibrotic kidneys as a therapeutic strategy to impede the progression of kidney fibrosis (Figure 9).

Previous studies have revealed that the expression of MCM6 in healthy tissues or paracarcinoma tissue is low, but its expression is upregulated in multiple cancer cells in association with cell cycle, proliferation, immune response, and maintenance of the DNA replication system.[27–29] In addition, MCM6 is a member of the MCM2-7 complex, which exerts an essential role for DNA synthesis.[18] Therefore, we wonder whether changes in MCM6 expression affect the stoichiometry of the MCM complex and the cell-cycle progression. As shown in Figure S2, knocking down of MCM6 expression strikingly decreased the expression of other MCM components (MCM2, MCM3, MCM4, MCM5, and MCM7), which might be attributed to the disability of MCM2-7 complex. Moreover, to explore the effect of MCM6 expression on cell cycle, we detected Ki67 level in UIRI mice and found that the number of Ki67-positive cells in the kidneys of UIRI mice was decreased by MCM6 knockdown, whereas increased by MCM6 overexpression (Figures 3B and S3A), suggesting that the expression of MCM6 affected general proliferative activity in the injured kidneys. Furthermore, we found that MCM6 deficiency contributed to G1 phase arrest by flow cytometry (Figures 3D and S3C), suggesting an important role of MCM6 in controlling G1 to S phase transition. However, cell-cycle arrest at G2/M phase has been considered as the pivotal factor in the development renal fibrosis.[30,31] And the reciprocal loop between partial EMT and G2/M arrest of TECs during renal fibrogenesis was reported.[7,32] Given the results that MCM6 has been associated with G1 phase arrest, the major functional role of MCM6 in the progression of renal fibrosis may not relate to cell-cycle arrest, but its role in the regulation of proliferative activity of TECs and tubular partial EMT progress seems clear.

In addition, it was reported that MCM6 promoted the migration and invasive ability of tumor cells by regulating the EMT cascade.[21] The tubular EMT program plays an important role in renal fibrosis; therefore, we wonder whether MCM6 contributes to renal fibrogenesis by regulating tubular partial EMT. To verify our hypotheses, two well-established experimental mouse models of UUO and UIRI were used *in vivo*, and TGF-β1- or H/R-stimulated TECs were used *in vitro* in this study. The upregulation of MCM6 was observed in the tubulointerstitium of fibrotic kidneys, as well as in cultured TECs in response to fibrotic stimulations. To explore the specific role of MCM6 in renal fibrosis, AAV harboring MCM6 was delivered into mouse kidneys to knockdown or overexpress MCM6 in renal tubules before establishing the UUO or UIRI model. Surprisingly, inhibition of MCM6 in the renal tubules further aggravated the partial EMT process and renal fibrosis in UUO and UIRI mice; however, overexpression of MCM6 markedly attenuated UUO- or UIRI-induced renal fibrosis. Based on these findings, the role of MCM6 in partial EMT program and renal fibrogenesis warrants attention in future studies.

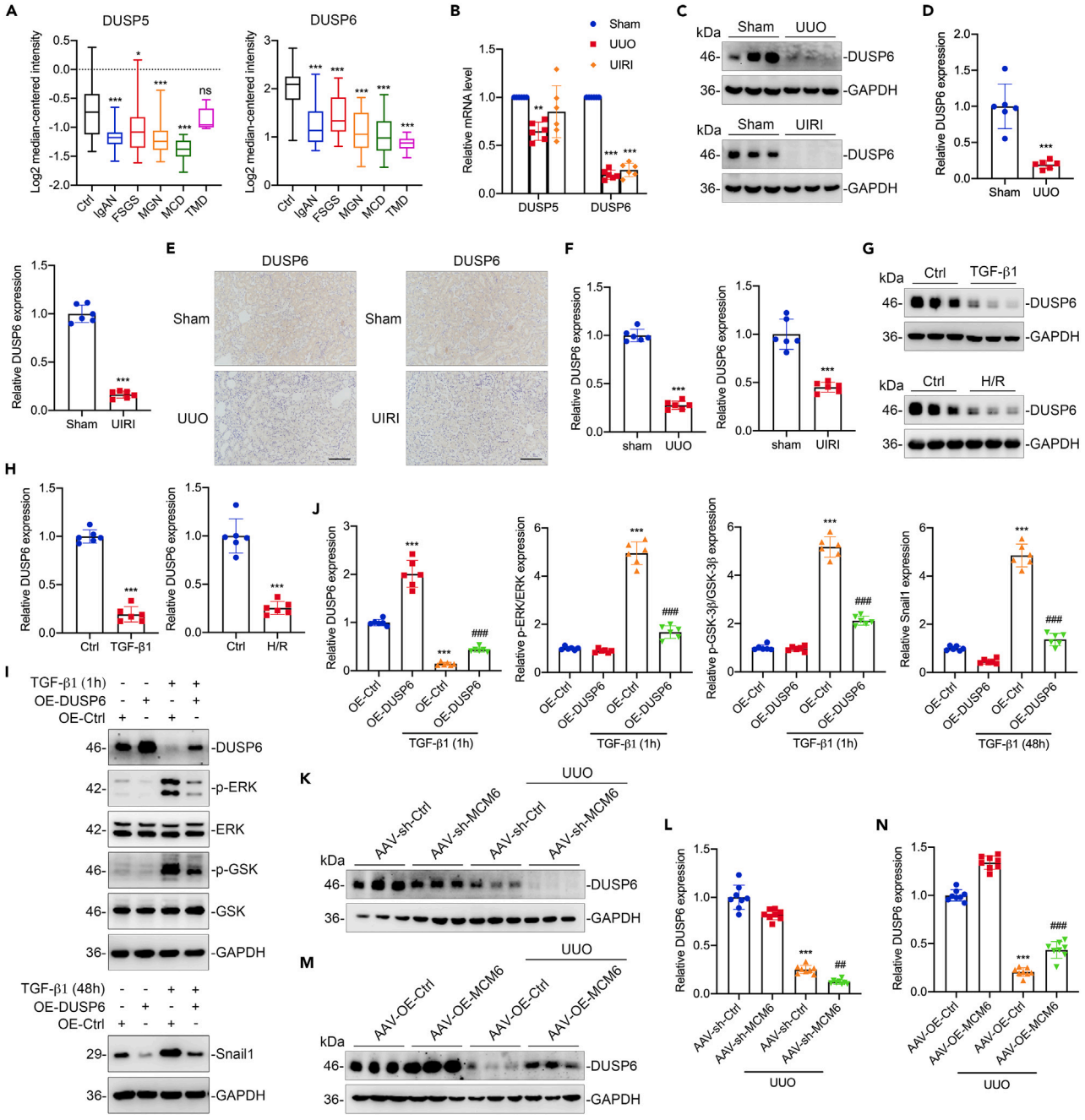

Figure 8. DUSP6 was involved in MCM6-induced renal fibrosis

(A) Graphical representation showing the relative expression patterns of DUSP5 and DUSP6 in patients with CKD. The data are obtained from the Nephroseq website. Ctrl, control samples from nephrectomized patients; IgAN, IgA nephropathy; FSGS, focal segmental glomerulosclerosis; MGN, membranous glomerulonephropathy; MCD, minimal change disease; TMD, thin basement membrane disease. *$p < 0.05$, ***$p < 0.001$ versus Ctrl group.

(B) Graphical representation showing the mRNA levels of DUSP5 and DUSP6 in the fibrotic kidney of mice with UUO and UIRI. n = 6 mice per group. ***$p < 0.001$ versus sham group.

(C and D) Representative western blots and summarized data showing the renal expression of DUSP6 in UUO- and UIRI-induced mice. n = 6 mice per group. ***$p < 0.001$ versus sham group.

(E and F) Immunohistochemical staining showing the expression of MCM6 in UUO models. Scale bar, 50 μm.

(G and H) Representative western blots and summarized data showing the expression of DUSP6 in TECs in response to TGF-β1 or H/R stimulation. n = 6. ***$p < 0.001$ versus Ctrl group.

Figure 8. *Continued*

(I and J) Representative western blots and summarized data showing the expression of ERK, phospho-ERK, GSK-3β, phospho-GSK-3β, and Snail1 in four groups, as indicated. TECs were transfected with OE-Ctrl or OE-DUSP6 plasmids for 48 h and then treated with TGF-β1 for 1 h or 48 h. n = 6. ***$p < 0.001$ versus OE-Ctrl, $^{###}p < 0.001$ versus OE-Ctrl + TGF-β1 (1 h or 48 h).

(K and L) Representative western blots and summarized data showing the expression of DUSP6 in four groups, as indicated. n = 8 mice per group. ***$p < 0.001$ versus AAV-sh-Ctrl group, $^{##}p < 0.01$ versus AAV-sh-Ctrl + UUO group.

(M and N) Representative western blots and summarized data showing the expression of DUSP6 in four groups, as indicated. n = 8 mice per group. ***$p < 0.001$ versus AAV-OE-Ctrl group, $^{###}p < 0.001$ versus AAV-OE-Ctrl + UUO group. All data are graphed as mean ± SEM.

Next, we sought to determine the possible regulatory mechanism of MCM6 in partial EMT program. Some studies have reported that MCM6 expression was associated with MEK/ERK signaling and PI3K/AKT/GSK-3β signaling in tumorigenicity and metastasis.[21,33] Multiple signaling pathways such as TGF-β/WNT, PI3K/AKT, p38 MAPK, ERK/MAPK, Jun N-terminal kinase, and Notch cooperate in the initiation and progression of EMT; some of these pathways often activate Snail1, which is a prominent transcription factor of EMT.[10] GSK-3β, a negative regulator of Snail1, promotes Snail stabilization, nuclear translocation, and subsequent EMT induction.[12] ERK suppresses GSK-3β activation, eventually leading to Snail nuclear retention and promotion of mesenchymal phenotypic changes.[34] Based on these studies, we mainly focused on the role of MCM6 in the regulation of ERK/GSK-3β/Snail1 signaling in tubular partial EMT progress. We found that phospho-ERK, phospho-GSK, and Snail1 levels were upregulated in fibrotic kidneys of UUO mice, and these increases were further increased by MCM6 knockdown; however, these increases were significantly inhibited by MCM6 overexpression. *In vitro* experiments also clarified the negative regulatory effect of MCM6 on ERK/GSK-3β/Snail1 signaling. To further verify the involvement of ERK/GSK-3β/Snail1 signaling in MCM6-induced tubular EMT, U0126 (a MEK1/2 inhibitor) and SB216763 (a GSK-3β inhibitor) were used alone or combined to block ERK signaling and GSK-3beta activity. We found that MCM6-induced GSK-3β phosphorylation was abolished by the MEK inhibitor, implying that MEK/ERK signaling is required for MCM6-induced inactivation of GSK-3β. In addition, both the MEK and the GSK-3β inhibitors significantly attenuated the expression of Snail1 in TECs with MCM6 deficiency, and the combination of two inhibitor further suppressed the expression of Snail1, indicating the role of ERK signaling and GSK-3beta activity in the regulation of MCM6-induced Snail1 expression. In our study, we concentrated on the correlation between MCM6 and ERK/GSK-3β/Snail1 signaling and showed positive results; however, multiple molecular pathways are involved in renal fibrogenesis, and the exact function of MCM6 in renal fibrosis still needs further exploration.

DUSPs are also known as MAPK-specific phosphatases and are classified into typical and atypical DUSPs according to their structural discrepancy. Based on the expression level in normal kidney tissues, they can be arbitrarily divided into 4 groups: high expression, moderate expression, low expression, and unexpressed groups.[24] Reduced DUSP1, DUSP4, DUSP6, DUSP10, and DUSP26 expression has been reported in diabetic nephropathy.[35–37] DUSP1 and DUSP5 are downregulated in hypertensive nephropathy,[38,39] DUSP1 is decreased in acute kidney injury,[40] and DUSP1 and DUSP4 are upregulated in CKD.[41,42] However, the expression and function of DUSP6 as a negative regulator of ERK signaling in renal fibrosis remain unclear. In this study, we detected the expression of DUSP6 in a various type of human CKD and, for the first time, identified that the expression of DUSP6 was substantially decreased in fibrotic kidneys of UUO or UIRI mice and cultured TECs in response to TGF-β1 or H/R stimulation, suggesting a potential role of DUSP6 in renal fibrogenesis. And we further revealed the involvement of MCM6 in the regulation of ERK/GSK-3β/Snail1 signaling. Given the evidence that DUSP6 and MCM6 are both involved in ERK/GSK-3β/Snail1 signaling, there is a reason to hypothesize that MCM6 may regulate DUSP6 expression, contribute to the activation of ERK/GSK-3β/Snail1 signaling, and then push forward the progress of renal fibrosis. To validate our hypothesis, we detected DUSP6 levels under MCM6 deficiency or overexpression conditions and found that MCM6 deficiency further downregulated the expression of DUSP6 in UUO-induced renal fibrosis; however, overexpression of MCM6 obviously reversed the decrease in DUSP6 in fibrotic kidneys. Although no direct evidence exists that MCM6 regulates ERK signaling via DUSP6, our results provide indications of the role of DUSP6 in MCM6-induced renal fibrosis; the specific regulatory mechanism of DUSP6 needs to be further investigated. Moreover, the expression patterns and function of DUSP6 in other kidney diseases require further exploration, particularly in disease models.

In conclusion, to the best of our knowledge, our results are the first to identify the upregulation of MCM6 in fibrotic kidneys and further provide direct evidence that MCM6 plays an important role in maintaining the tubular epithelial phenotype and protecting against renal fibrosis. More importantly, we demonstrated that the ERK/GSK-3β/Snail1 signaling pathway may be a key pathway linking MCM6 to the regulation of the tubular partial EMT program, ECM accumulation, and myofibroblast activation in renal fibrogenesis. Although further studies are needed, our findings highlight the potential of MCM6 as a therapeutic target for the treatment of renal fibrosis. Targeting DUSP6-mediated ERK/GSK-3β/Snail1 signaling might be a plausible therapeutic strategy to disrupt tubular partial EMT progress, therefore alleviating renal fibrosis.

Limitations of the study

Tubular-specific MCM6 knockout mice would represent the ideal model to investigate the specific role of MCM6 in renal fibrosis *in vivo*. However, owing to the lack of such a knockout mouse model, the exact role and regulatory mechanisms of MCM6 in renal fibrogenesis remain to be further elucidated. In addition, we discovered the dysregulated DUSP6 activity in MCM6 knockdown kidneys, but there was an unclear mechanistic link between MCM6 and DUSP6 signaling in regulating outcomes after kidney injury. Therefore, future studies should explore the specific regulatory mechanism of MCM6 in the regulation of DUSP6. In our study, dissection of tissues was carried

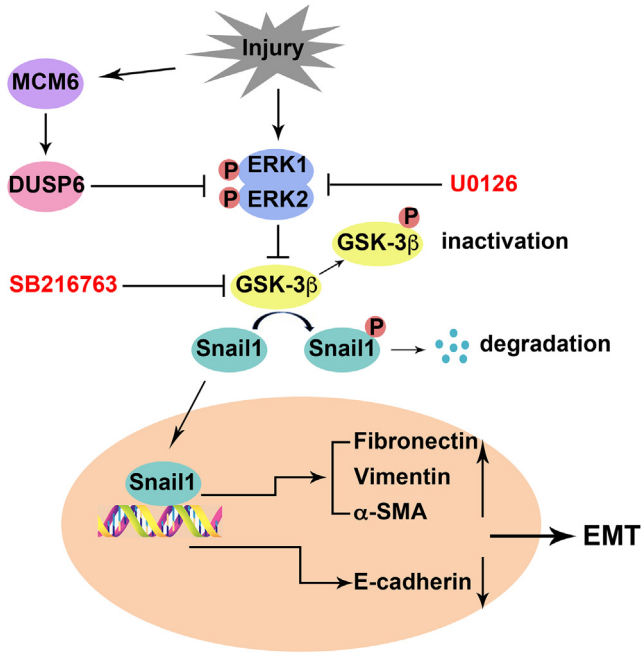

Figure 9. Hypothetical model showing the role of MCM6 in renal fibrosis

Tubular injury triggers the upregulation of MCM6 in proximal TECs. MCM6 deficiency potentiates signal transduction and activates ERK/GSK-3β/Snail1 signaling, contributing to tubular EMT program, extracellular matrix deposition, and myofibroblast activation before eventually leading to renal fibrosis. DUSP6 may be involved in MCM6-induced renal fibrosis by regulating ERK phosphorylation.

out at 7 days after UUO or UIRI operation for investigating the functional role of MCM6 in the early stage of renal fibrosis; the potential of MCM6 in longer recovery from UUO or UIRI should be conducted in future experiments. To maintain hormonal stability and reduce variability, male mice were used in this study. Future studies will be needed to consider the possibility of the effect of MCM6 on gender in patients with CKD.

STAR★METHODS

Detailed methods are provided in the online version of this paper and include the following:

- KEY RESOURCES TABLE
- RESOURCE AVAILABILITY
  - Lead contact
  - Materials availability
  - Data and code availability
- EXPERIMENTAL MODEL AND STUDY PARTICIPANT DETAILS
  - Animals
  - Cell line
- METHODS DETAILS
  - Intrarenal adeno-associated virus delivery
  - Histology and immunohistochemistry
  - Immunofluorescence staining
  - Cell treatment and transfection
  - Western blotting
  - RNA extraction and quantitative real-time PCR (qRT-PCR)
- QUANTIFICATION AND STATISTICAL ANALYSIS

SUPPLEMENTAL INFORMATION

Supplemental information can be found online at https://doi.org/10.1016/j.isci.2023.107940.

ACKNOWLEDGMENTS

This study was financially supported by the National Natural Science Foundation of China (81974096, 82170773, 81961138007, and 81974097), the National Key Research and Development Program (2018YFC1314000), the Program for HUST Academic Frontier Youth Team (2017QYTD20), and the Fundamental Research Funds for the Central Universities (HUST: 2022JYCXJJ047).

AUTHOR CONTRIBUTIONS

J. Huang designed the study and wrote the manuscript. J. Huang, Z.-F. Xu, F. Liu, and A.-N. Song performed the experiments and analyzed the data. C. Zhang and H. Su supervised the study and provided a series of experimental instructions and help. All authors approved the final manuscript.

DECLARATION OF INTERESTS

All authors declare that they have no conflict of interest.

INCLUSION AND DIVERSITY

We support inclusive, diverse, and equitable conduct of research.

Received: April 19, 2023
Revised: August 2, 2023
Accepted: September 13, 2023
Published: September 16, 2023

REFERENCES

1. Romagnani, P., Remuzzi, G., Glassock, R., Levin, A., Jager, K.J., Tonelli, M., Massy, Z., Wanner, C., and Anders, H.J. (2017). Chronic kidney disease. Nat. Rev. Dis. Primers *3*, 17088. https://doi.org/10.1038/nrdp.2017.88.
2. Hu, L., Ding, M., and He, W. (2021). Emerging Therapeutic Strategies for Attenuating Tubular EMT and Kidney Fibrosis by Targeting Wnt/β-Catenin Signaling. Front. Pharmacol. *12*, 830340. https://doi.org/10.3389/fphar.2021.830340.
3. Wang, J., Li, J., Zhang, X., Zhang, M., Hu, X., and Yin, H. (2022). Molecular mechanisms of histone deacetylases and inhibitors in renal fibrosis progression. Front. Mol. Biosci. *9*, 986405. https://doi.org/10.3389/fmolb.2022.986405.
4. Xu, Z., Zhang, M., Wang, Y., Chen, R., Xu, S., Sun, X., Yang, Y., Lin, Z., Wang, S., and Huang, H. (2022). Gentiopicroside Ameliorates Diabetic Renal Tubulointerstitial Fibrosis via Inhibiting the AT1R/CK2/NF-κB Pathway. Front. Pharmacol. *13*, 848915. https://doi.org/10.3389/fphar.2022.848915.
5. Liu, B.C., Tang, T.T., Lv, L.L., and Lan, H.Y. (2018). Renal tubule injury: a driving force toward chronic kidney disease. Kidney Int. *93*, 568–579. https://doi.org/10.1016/j.kint.2017.09.033.
6. Grande, M.T., Sánchez-Laorden, B., López-Blau, C., De Frutos, C.A., Boutet, A., Arévalo, M., Rowe, R.G., Weiss, S.J., López-Novoa, J.M., and Nieto, M.A. (2015). Snail1-induced partial epithelial-to-mesenchymal transition drives renal fibrosis in mice and can be targeted to reverse established disease. Nat. Med. *21*, 989–997. https://doi.org/10.1038/nm.3901.
7. Lovisa, S., LeBleu, V.S., Tampe, B., Sugimoto, H., Vadnagara, K., Carstens, J.L., Wu, C.C., Hagos, Y., Burckhardt, B.C., Pentcheva-Hoang, T., et al. (2015). Epithelial-to-mesenchymal transition induces cell cycle arrest and parenchymal damage in renal fibrosis. Nat. Med. *21*, 998–1009. https://doi.org/10.1038/nm.3902.
8. Canaud, G., and Bonventre, J.V. (2015). Cell cycle arrest and the evolution of chronic kidney disease from acute kidney injury. Nephrol. Dial. Transplant. *30*, 575–583. https://doi.org/10.1093/ndt/gfu230.
9. Wynn, T.A. (2010). Fibrosis under arrest. Nat. Med. *16*, 523–525. https://doi.org/10.1038/nm0510-523.
10. Lamouille, S., Xu, J., and Derynck, R. (2014). Molecular mechanisms of epithelial-mesenchymal transition. Nat. Rev. Mol. Cell Biol. *15*, 178–196. https://doi.org/10.1038/nrm3758.
11. Barrallo-Gimeno, A., and Nieto, M.A. (2005). The Snail genes as inducers of cell movement and survival: implications in development and cancer. Development *132*, 3151–3161. https://doi.org/10.1242/dev.01907.
12. Zhou, B.P., Deng, J., Xia, W., Xu, J., Li, Y.M., Gunduz, M., and Hung, M.C. (2004). Dual regulation of Snail by GSK-3beta-mediated phosphorylation in control of epithelial-mesenchymal transition. Nat. Cell Biol. *6*, 931–940. https://doi.org/10.1038/ncb1173.
13. Yook, J.I., Li, X.Y., Ota, I., Hu, C., Kim, H.S., Kim, N.H., Cha, S.Y., Ryu, J.K., Choi, Y.J., Kim, J., et al. (2006). A Wnt-Axin2-GSK3beta cascade regulates Snail1 activity in breast cancer cells. Nat. Cell Biol. *8*, 1398–1406. https://doi.org/10.1038/ncb1508.
14. Sahlgren, C., Gustafsson, M.V., Jin, S., Poellinger, L., and Lendahl, U. (2008). Notch signaling mediates hypoxia-induced tumor cell migration and invasion. Proc. Natl. Acad. Sci. USA *105*, 6392–6397. https://doi.org/10.1073/pnas.0802047105.
15. Wu, Y., Deng, J., Rychahou, P.G., Qiu, S., Evers, B.M., and Zhou, B.P. (2009). Stabilization of snail by NF-kappaB is required for inflammation-induced cell migration and invasion. Cancer Cell *15*, 416–428. https://doi.org/10.1016/j.ccr.2009.03.016.
16. Li, S., Lu, J., Chen, Y., Xiong, N., Li, L., Zhang, J., Yang, H., Wu, C., Zeng, H., and Liu, Y. (2017). MCP-1-induced ERK/GSK-3β/Snail signaling facilitates the epithelial-mesenchymal transition and promotes the migration of MCF-7 human breast carcinoma cells. Cell. Mol. Immunol. *14*, 621–630. https://doi.org/10.1038/cmi.2015.106.
17. Zhai, Y., Cheng, E., Wu, H., Li, N., Yung, P.Y.K., Gao, N., and Tye, B.K. (2017). Open-ringed structure of the Cdt1-Mcm2-7 complex as a precursor of the MCM double hexamer. Nat. Struct. Mol. Biol. *24*, 300–308. https://doi.org/10.1038/nsmb.3374.
18. Saleh, A., Noguchi, Y., Aramayo, R., Ivanova, M.E., Stevens, K.M., Montoya, A., Sunidhi, S., Carranza, N.L., Skwark, M.J., and Speck, C. (2022). The structural basis of Cdc7-Dbf4 kinase dependent targeting and phosphorylation of the MCM2-7 double hexamer. Nat. Commun. *13*, 2915. https://doi.org/10.1038/s41467-022-30576-1.
19. Zhang, J., Zhang, H., Wang, Y., and Wang, Q. (2021). MCM2-7 in Clear Cell Renal Cell Carcinoma: MCM7 Promotes Tumor Cell Proliferation. Front. Oncol. *11*, 782755. https://doi.org/10.3389/fonc.2021.782755.
20. Liu, Z., Li, J., Chen, J., Shan, Q., Dai, H., Xie, H., Zhou, L., Xu, X., and Zheng, S. (2018). MCM family in HCC: MCM6 indicates adverse tumor features and poor outcomes and promotes S/G2 cell cycle progression. BMC Cancer *18*, 200. https://doi.org/10.1186/s12885-018-4056-8.
21. Liu, M., Hu, Q., Tu, M., Wang, X., Yang, Z., Yang, G., and Luo, R. (2018). MCM6 promotes metastasis of hepatocellular carcinoma via MEK/ERK pathway and serves as a novel serum biomarker for early recurrence. J. Exp. Clin. Cancer Res. *37*, 10. https://doi.org/10.1186/s13046-017-0669-z.
22. Zheng, T., Chen, M., Han, S., Zhang, L., Bai, Y., Fang, X., Ding, S.Z., and Yang, Y. (2014). Plasma minichromosome maintenance complex component 6 is a novel biomarker

for hepatocellular carcinoma patients. Hepatol. Res. *44*, 1347–1356. https://doi.org/10.1111/hepr.12303.

23. Airik, M., Phua, Y.L., Huynh, A.B., McCourt, B.T., Rush, B.M., Tan, R.J., Vockley, J., Murray, S.L., Dorman, A., Conlon, P.J., and Airik, R. (2022). Persistent DNA damage underlies tubular cell polyploidization and progression to chronic kidney disease in kidneys deficient in the DNA repair protein FAN1. Kidney Int. *102*, 1042–1056. https://doi.org/10.1016/j.kint.2022.07.003.
24. Li, H., Xiong, J., Du, Y., Huang, Y., and Zhao, J. (2022). Dual-Specificity Phosphatases and Kidney Diseases. Kidney Dis. *8*, 13–25. https://doi.org/10.1159/000520142.
25. Kidger, A.M., Saville, M.K., Rushworth, L.K., Davidson, J., Stellzig, J., Ono, M., Kuebelsbeck, L.A., Janssen, K.P., Holzmann, B., Morton, J.P., et al. (2022). Suppression of mutant Kirsten-RAS (KRAS(G12D))-driven pancreatic carcinogenesis by dual-specificity MAP kinase phosphatases 5 and 6. Oncogene *41*, 2811–2823. https://doi.org/10.1038/s41388-022-02302-0.
26. Zeng, T., Guan, Y., Li, Y.K., Wu, Q., Tang, X.J., Zeng, X., Ling, H., and Zou, J. (2021). The DNA replication regulator MCM6: An emerging cancer biomarker and target. Clin. Chim. Acta *517*, 92–98. https://doi.org/10.1016/j.cca.2021.02.005.
27. Vigouroux, C., Casse, J.M., Battaglia-Hsu, S.F., Brochin, L., Luc, A., Paris, C., Lacomme, S., Gueant, J.L., Vignaud, J.M., and Gauchotte, G. (2015). Methyl(R217)HuR and MCM6 are inversely correlated and are prognostic markers in non small cell lung carcinoma. Lung Cancer *89*, 189–196. https://doi.org/10.1016/j.lungcan.2015.05.008.
28. Yuan, Z., Schneider, S., Dodd, T., Riera, A., Bai, L., Yan, C., Magdalou, I., Ivanov, I., Stillman, B., Li, H., and Speck, C. (2020). Structural mechanism of helicase loading onto replication origin DNA by ORC-Cdc6. Proc. Natl. Acad. Sci. USA. *117*, 17747–17756. https://doi.org/10.1073/pnas.2006231117.
29. Forsburg, S.L. (2004). Eukaryotic MCM proteins: beyond replication initiation. Microbiol. Mol. Biol. Rev. *68*, 109–131. https://doi.org/10.1128/mmbr.68.1.109-131.2004.
30. Yang, L., Besschetnova, T.Y., Brooks, C.R., Shah, J.V., and Bonventre, J.V. (2010). Epithelial cell cycle arrest in G2/M mediates kidney fibrosis after injury. Nat. Med. *16*, 535–543. 531p following 143. https://doi.org/10.1038/nm.2144.
31. Zhang, Y., Yang, Y., Yang, F., Liu, X., Zhan, P., Wu, J., Wang, X., Wang, Z., Tang, W., Sun, Y., et al. (2023). HDAC9-mediated epithelial cell cycle arrest in G2/M contributes to kidney fibrosis in male mice. Nat. Commun. *14*, 3007. https://doi.org/10.1038/s41467-023-38771-4.
32. Qi, R., Wang, J., Jiang, Y., Qiu, Y., Xu, M., Rong, R., and Zhu, T. (2021). Snai1-induced partial epithelial-mesenchymal transition orchestrates p53-p21-mediated G2/M arrest in the progression of renal fibrosis via NF-κB-mediated inflammation. Cell Death Dis. *12*, 44. https://doi.org/10.1038/s41419-020-03322-y.
33. Wang, Y., Chen, H., Liu, W., Yan, H., Zhang, Y., Cheung, A.H.K., Zhang, J., Chen, B., Liang, L., Zhou, Z., et al. (2022). MCM6 is a critical transcriptional target of YAP to promote gastric tumorigenesis and serves as a therapeutic target. Theranostics *12*, 6509–6526. https://doi.org/10.7150/thno.75431.
34. Gong, K., Zhou, F., Huang, H., Gong, Y., and Zhang, L. (2012). Suppression of GSK3β by ERK mediates lipopolysaccharide induced cell migration in macrophage through β-catenin signaling. Protein Cell *3*, 762–768. https://doi.org/10.1007/s13238-012-2058-x.
35. Denhez, B., Rousseau, M., Dancosst, D.A., Lizotte, F., Guay, A., Auger-Messier, M., Côté, A.M., and Geraldes, P. (2019). Diabetes-Induced DUSP4 Reduction Promotes Podocyte Dysfunction and Progression of Diabetic Nephropathy. Diabetes *68*, 1026–1039. https://doi.org/10.2337/db18-0837.
36. Sheng, J., Li, H., Dai, Q., Lu, C., Xu, M., Zhang, J., and Feng, J. (2019). DUSP1 recuses diabetic nephropathy via repressing JNK-Mff-mitochondrial fission pathways. J. Cell. Physiol. *234*, 3043–3057. https://doi.org/10.1002/jcp.27124.
37. Chen, L., Wang, Y., Luan, H., Ma, G., Zhang, H., and Chen, G. (2020). DUSP6 protects murine podocytes from high glucose-induced inflammation and apoptosis. Mol. Med. Rep. *22*, 2273–2282. https://doi.org/10.3892/mmr.2020.11317.
38. Chen, X., Cao, Y., Wang, Z., Zhang, D., and Tang, W. (2019). Bioinformatic analysis reveals novel hub genes and pathways associated with hypertensive nephropathy. Nephrology *24*, 1103–1114. https://doi.org/10.1111/nep.13508.
39. Zhang, C., He, X., Murphy, S.R., Zhang, H., Wang, S., Ge, Y., Gao, W., Williams, J.M., Geurts, A.M., Roman, R.J., and Fan, F. (2019). Knockout of Dual-Specificity Protein Phosphatase 5 Protects Against Hypertension-Induced Renal Injury. J. Pharmacol. Exp. Ther. *370*, 206–217. https://doi.org/10.1124/jpet.119.258954.
40. Jung, Y.J., Park, W., Kang, K.P., and Kim, W. (2020). SIRT2 is involved in cisplatin-induced acute kidney injury through regulation of mitogen-activated protein kinase phosphatase-1. Nephrol. Dial. Transplant. *35*, 1145–1156. https://doi.org/10.1093/ndt/gfaa042.
41. Li, Z., Liu, X., Tian, F., Li, J., Wang, Q., and Gu, C. (2018). MKP2 inhibits TGF-β1-induced epithelial-to-mesenchymal transition in renal tubular epithelial cells through a JNK-dependent pathway. Clin. Sci. *132*, 2339–2355. https://doi.org/10.1042/cs20180602.
42. Wahab, N., Cox, D., Witherden, A., and Mason, R.M. (2007). Connective tissue growth factor (CTGF) promotes activated mesangial cell survival via up-regulation of mitogen-activated protein kinase phosphatase-1 (MKP-1). Biochem. J. *406*, 131–138. https://doi.org/10.1042/bj20061817.
43. Tang, H., Su, H., Fan, D., Ye, C., Lei, C.T., Jiang, H.J., Gao, P., He, F.F., and Zhang, C. (2016). MAD2B-mediated SnoN downregulation is implicated in fibroblast activation and tubulointerstitial fibrosis. Am. J. Physiol. Renal Physiol. *311*, F207–F216. https://doi.org/10.1152/ajprenal.00600.2015.
44. Huang, J., Bao, D., Lei, C.T., Tang, H., Zhang, C.Y., Su, H., and Zhang, C. (2020). Selenoprotein T protects against cisplatin-induced acute kidney injury through suppression of oxidative stress and apoptosis. Faseb j *34*, 11983–11996. https://doi.org/10.1096/fj.202000180RR.

STAR★METHODS

KEY RESOURCES TABLE

REAGENT or RESOURCE	SOURCE	IDENTIFIER
Antibodies		
Anti-MCM6	Abcam	Cat# ab201683; RRID: AB_2924827
anti-Fibronectin	Sigma-Aldrich	Cat# F3648; RRID: AB_476976
anti-Vimentin	Cell Signaling Technology	Cat# 5741; RRID: AB_10695459
anti-α-SMA	Proteintech	Cat# 14395-1-AP; RRID: AB_2223009
anti-E-cadherin	Proteintech	Cat# 20874-1-AP; RRID: AB_10697811
anti-phospho-ERK	Cell Signaling Technology	Cat# 4370; RRID: AB_2315112
anti-ERK	Cell Signaling Technology	Cat# 4695; RRID: AB_390779
anti-phospho-GSK-3β	Cell Signaling Technology	Cat# 5558; RRID: AB_10013750
anti-GSK-3β	Cell Signaling Technology	Cat# 12456; RRID: AB_2636978
anti-Snail1	Proteintech	Cat# 14395-1-AP; RRID: AB_2223009
anti-DUSP6	Abcam	Cat# ab76310; RRID: AB_1523517
anti-Lotus Tetragonolobus Lectin	Vector Laboratories	Cat# FL-1321, RRID: AB_2336559
anti-GAPDH	Proteintech	Cat# 10494-1-AP; RRID: AB_2263076
Bacterial and virus strains		
Adeno-associated viral vectors harboring MCM6 (AAV-sh-MCM6)	Vigenebio	N/A
Adeno-associated viral vectors harboring MCM6 (AAV-OE-MCM6)	Vigenebio	N/A
Chemicals, peptides, and recombinant proteins		
High-glucose DMEM medium	Gibco	Cat#C12430500BT
Fetal bovine serum	Gibco	Cat#10099-141C
Penicillin-streptomycin solution	Sigma-Aldrich	Cat#P4333
RIPA buffer	Beyotime	Cat#P0013B
PVDF membranes	Millipore	Cat#IPVH00010
Triton X-100	Servicebio	Cat#GC204003
RNAiso Plus	Takara	Cat#D9108A
Hematoxylin	Solarbio	Cat#G1120
DAPI	Servicebio	Cat#G1012
Recombinant human transforming growth factor β1	R&D Systems	Cat#7754-BH
U0126	Selleck Chemical	Cat#1173097-76-1
SB216763	Selleck Chemical	CAt#280744-09-4
Lipofectamine 2000	Invitrogen	Cat#11668019
Critical commercial assays		
PrimeScript RT Master Mix	Takara	Cat#RR036A
SYBR Green PCR kit	Takara	Cat#RR820A
DAB kit	Servicebio	Cat#G1212

(*Continued on next page*)

Continued

REAGENT or RESOURCE	SOURCE	IDENTIFIER
Experimental models: Cell lines		
Rat renal proximal TECs (NRK-52E)	ATCC	RRID: CVCL_0468
Human renal proximal TECs (HK-2)	ATCC	RRID: CVCL_0302
Experimental models: Organisms/strains		
Mouse: *C57BL/6J*	Charles River	N/A
Oligonucleotides		
siRNA targeting sequence of MCM6; 5′-ACGGCAATGATGAAGTAAA-3′	This paper	N/A
Forward primer for mouse MCM2; GTCAGCTCTATCTCGTCCCC	This paper	N/A
Reverse primer for mouse MCM2; ATCAGAACTACCAACGTATCCGC	This paper	N/A
Forward primer for mouse MCM3; AGCGCAGAGAGACTACTTGGA	This paper	N/A
Reverse primer for mouse MCM3; GCGGTTAGCCCTCTTTTCATTC	This paper	N/A
Forward primer for mouse MCM4; TTTGTGCGCGTTTGCAACTA	This paper	N/A
Reverse primer for mouse MCM4; GTGACGACCTGCTTTCCTCA	This paper	N/A
Forward primer for mouse MCM5; TCTAGGAGGGCTGAGGTACAG	This paper	N/A
Reverse primer for mouse MCM5; ACTCCTTGAATCGCCTCTGC	This paper	N/A
Forward primer for mouse MCM6; GAATCATTGGGGAGCGGTCA	This paper	N/A
Reverse primer for mouse MCM6; GACACCACAAAAAGCCCACC	This paper	N/A
Forward primer for mouse MCM7; TCGGAGATAGCTGCAGTAGAAA	This paper	N/A
Reverse primer for mouse MCM7; TTGAGTCGACCAACTCAGGGT	This paper	N/A
Forward primer for mouse DUSP5; AGCGTGGTCTCTCCCAACTT	This paper	N/A
Reverse primer for mouse DUSP5; GGTACGGAATGTGCAGTAGGT	This paper	N/A
Forward primer for mouse DUSP6; ATAGATACGCTCAGACCCGTG	This paper	N/A
Reverse primer for mouse DUSP6; ATCAGCAGAAGCCGTTCGTT	This paper	N/A
Forward primer for mouse GAPDH; TGGCCTTCCGTGTTCCTAC	This paper	N/A
Reverse primer for mouse GAPDH; GAGTTGCTGTTGAAGTCGCA	This paper	N/A
Forward primer for Rattus MCM6; CGATGCTTGGGGACAGTTGA	This paper	N/A
Reverse primer for Rattus MCM6; CAGGACAAGCACAAAGTGCC	This paper	N/A

(*Continued on next page*)

Continued

REAGENT or RESOURCE	SOURCE	IDENTIFIER
Forward primer for Rattus Fibronectin; CCCTTCCACACCCCAATCTT	This paper	N/A
Reverse primer for Rattus Fibronectin; ACTGGGTTGTTGGTGGGATG	This paper	N/A
Forward primer for Rattus Vimentin; GCAGCCTCTATTCCTCGTCC	This paper	N/A
Reverse primer for Rattus Vimentin; GAAGCGGTCATTCAGCTCCT	This paper	N/A
Forward primer for Rattus a-SMA; TTGTCCACCGCAAATGCTTC	This paper	N/A
Reverse primer for Rattus a-SMA; TGAAGGCGCTGATCCACAAA	This paper	N/A
Forward primer for Rattus GAPDH; GCATCTTCTTGTGCAGTGCC	This paper	N/A
Reverse primer for Rattus GAPDH; TACGGCCAAATCCGTTCACA	This paper	N/A
Recombinant DNA		
GFP-RFP-DUSP6 plasmid	GeneChem	N/A
Software and algorithms		
ImageJ	National Institutes of Health	https://mirror.imagej.net
GraphPad Prism	GraphPad Software	https://www.graphpad.com

RESOURCE AVAILABILITY

Lead contact

Further information and requests for resources and reagents should be directed to and will be fulfilled by the lead contact, Chun Zhang (drzhangchun@hust.edu.cn).

Materials availability

Plasmids and adeno-associated viral generated in this study are available from the lead contact upon reasonable request with a completed Materials Transfer Agreement.

Data and code availability

- This paper does not report original code.
- This paper does not have any genomic or sequencing data.
- Any additional information required to reanalyze the data reported in this paper is available from the lead contact upon request.

EXPERIMENTAL MODEL AND STUDY PARTICIPANT DETAILS

Animals

C57BL/6J male mice (8 weeks old) were obtained from Charles River (Beijing, China). Mice were subjected to unilateral ureteral obstruction (UUO) or unilateral ischemic reperfusion injury (UIRI) surgery as described in previous studies.[43] To establish the UUO model, the left ureter of the mice was ligated using a 4-0 silk suture in a midline abdominal incision when the mice were under anesthesia with sodium pentobarbital. The mice were euthanized 7 days after UUO surgery and the kidney tissues were harvested for various analyses. For establishing the UIRI model, the left renal pedicle of the mice was clipped using a microaneurysm clamp for 35 min in a dorsal incision when the mice were under anesthesia with sodium pentobarbital. After inducing ischemia, the clamp was removed for reperfusion. During the ischemic period, the body temperature was maintained between 37°C and 38°C. And the mice were euthanized 7 days after UIRI surgery. Serum and renal tissues were harvested for experimental analyses.

All animal experiments were approved by the Animal Ethics Committee of the Huazhong University of Science and Technology ([2022] IACUC Number: 3033). The procedures were conducted in accordance with the Guide for the Care and Use of Laboratory Animals of the National Institute of Health (Bethesda, MD, USA).

Cell line

The rat renal proximal TEC cell line (NRK-52E) and human renal proximal TEC cell line (HK-2) were purchased from the American Type Culture Collection (Manassas, VA, USA). The cells were cultured in high-glucose DMEM medium (Gibco, USA) containing 10% fetal bovine serum (FBS) and 1% penicillin-streptomycin solution (Sigma-Aldrich, USA) at 37°C in a humidified incubator containing 5% CO2. Both of cell lines had been detected negative for mycoplasma contamination.

METHODS DETAILS

Intrarenal adeno-associated virus delivery

Two adeno-associated viral vectors harboring MCM6—AAV9 harboring MCM6 to knockdown MCM6 expression (AAV-sh-MCM6) and AAV9 harboring MCM6 to overexpress MCM6 expression (AAV-OE-MCM6)—were developed and obtained from Vigenebio (Shandong, China). The viruses were delivered to the mouse kidneys via intraparenchymal injection 30 days prior to the establishment of the UUO or UIRI model. Briefly, the mice were temporarily anesthetized and the abdominal cavity was opened to expose the bilateral kidneys. Then, 100 μL of MCM6 targeted-AAV9 or control AAV9 particles at a concentration of 8×10^{11} pfu/mL were slowly delivered into the renal cortex (5–6 sites) of the left kidney with a 31G needle. Approximately a month later, UUO or UIRI surgery was performed on the left kidney.

Histology and immunohistochemistry

Kidney tissues were fixed in 4% paraformaldehyde, embedded in paraffin, sectioned into 3 μm thick of sections, and stained with HE and Masson's trichrome according to the manufacturer's instructions. For immunohistochemical staining, the sections were incubated overnight at 4°C with the following primary antibodies: MCM6 (ab201683, Abcam, UK), anti-Fibronectin (F3648, Sigma-Aldrich, USA), anti-Vimentin (5741, Cell Signaling Technology, USA), anti-α-SMA (ab5694, Abcam, UK), and anti-DUSP6 (ab76310, Abcam, UK). This was followed by incubation with biotinylated secondary antibodies for 1 h at 37°C according to the standard protocol. After staining with 3,3′-Diaminobenzidine and counterstaining with hematoxylin, the density of the positively stained areas was calculated using Image-Pro Plus software.

Immunofluorescence staining

Kidney tissues were fixed in 4% paraformaldehyde, embedded in paraffin, sectioned in 4 mm slices. The cells and frozen tissue sections were fixed with 4% paraformaldehyde for 30 min, permeabilized with 0.3% Triton X-100 for 20 min, and blocked with 5% donkey serum for 1 h. The tissue samples were incubated overnight at 4°C with the following primary antibodies: anti-MCM6 (ab201683, Abcam, UK), anti-Fibronectin (F3648, Sigma-Aldrich, USA), anti-α-SMA (14395-1-AP, Proteintech, USA), anti-E-cadherin (20874-1-AP, Proteintech, USA), and anti-Lotus Tetragonolobus Lectin (LTL) (FL-1321, VECTOR Laboratories, USA). Alexa Fluor 488-conjugated donkey anti-rabbit and Alexa Fluor 594-conjugated donkey anti-mouse antibodies (Invitrogen, USA) were used as secondary antibodies. The nuclei were counterstained with DAPI (Beyotime Biotechnology, Shanghai, China) for 5 min. The images were captured using a confocal laser-scanning microscope.

Cell treatment and transfection

For transforming growth factor β1 (TGF-β1) treatment, NRK-52E cells were serum-starved for 12 h and then treated with recombinant human TGF-β1 (5 ng/mL; R&D Systems, Minneapolis, MN, USA) for indicated times. For hypoxia-reoxygenation (H/R) injury, TECs were cultured in the sugar-free DMEM medium (Gibco, USA) and incubated in a tri-gas incubator (94% N_2, 5% CO_2, and 1% O_2) at 37°C for 24 h. Subsequently, the cells were transferred to the normal conditions (5% CO_2 and 95% O_2) and incubated with fresh DMEM medium with 10% FBS at 37°C for 24 h for reoxygenations. For some experiments, the cultured cells were pre-treated with 30 μM U0126 (Selleck Chemical, Houston, USA) or 50 μM SB216763 (Selleck Chemicals, Houston, USA) before the treatment of TGF-β1 or H/R.

For siRNA transfection, specific siRNA targeting MCM6 (si-MCM6) or scramble siRNA (si-NC) (RiboBio, Guangzhou, China) were transfected into NRK-52E cells using Lipofectamine 2000 reagent (Invitrogen, Carlsbad, CA) according to the manufacturer's instructions. After culturing for 48 h, the knockdown efficiency of si-MCM6 was determined by immunoblotting and real-time PCR assay. The sequence of si-MCM6 was 5′-ACGGCAATGATGAAGTAAA-3′.

For plasmids transfection, DUSP6 overexpress plasmids or scramble plasmids (GeneChem, Shanghai, China) were transiently transfected into NRK-52E cells using Lipofectamine 2000 reagent (Invitrogen, Carlsbad, CA) according to the manufacturer's protocol. After culturing for 48 h, the overexpression efficiency of MCM6 was determined by immunoblotting assay.

Western blotting

Western blotting was performed as previously described.[44] Briefly, total cellular and tissue proteins were extracted using RIPA buffer (Beyotime Biotechnology, Shanghai, China), separated using SDS-PAGE, and transferred to PVDF membranes (Merck Millipore, MA, USA). The membranes were blocked with 5% milk for 1 h, incubated with primary antibody overnight at 4°C, incubated with secondary antibodies, and detected using enhanced chemiluminescence solution. The densities of the images were analyzed using ImageJ software (National Institutes of Health, Bethesda, MD, USA). The following primary antibodies were used in this study: MCM6 (ab201683, Abcam, UK), anti-Fibronectin (F3648, Sigma-Aldrich, USA), anti-α-SMA (14395-1-AP, Proteintech, USA), anti-E-cadherin (20874-1-AP, Proteintech, USA), anti-Vimentin (5741, Cell Signaling Technology, USA), and anti-phospho-ERK (4370, Cell Signaling Technology, USA), anti-ERK (4695, Cell Signaling

Technology, USA), anti-phospho-GSK-3β (5558, Cell Signaling Technology, USA), anti-GSK-3β (12456, Cell Signaling Technology, USA), anti-Snail1 (14395-1-AP, Proteintech, USA), anti-DUSP6 (ab76310, Abcam, UK), and anti-GAPDH (10494-1-AP, Proteintech, USA).

RNA extraction and quantitative real-time PCR (qRT-PCR)

Total RNA was extracted using the Trizol RNA isolation system (Takara, Dalian, China) and reverse transcribed into cDNA using PrimeScript RT Master Mix (RR036A, Takara) according to the manufacturer's instructions. The mRNA level target genes were measured using SYBR Premix Ex TaqTM (RR820A, Takara) on a StepOnePlus Real-Time PCR system as described previously.[44] Experiments were performed in triplicate. The primers used in this study are shown in Table 1.

QUANTIFICATION AND STATISTICAL ANALYSIS

All data are expressed as mean ± SEM. A t-test was used to compare two groups, and one-way analysis of variance followed by Duncan's multiple range test was used to compare more than two groups. $p < 0.05$ was considered statistically significant.